THE ROLE OF ENDOGENOUS RETINOIC ACID

IN JAW DEVELOPMENT

by

Churmy Yong Fan

B.Sc. The University of British Columbia, 2008

A THESIS SUBMITTED IN PARTIAL FULFILLMENT OF

THE REQUIREMENTS FOR THE DEGREE OF

MASTER OF SCIENCE

in

The Faculty of Graduate Studies

(Cell and Developmental Biology)

THE UNIVERSITY OF BRITISH COLUMBIA

(Vancouver)

September 2011

Abstract

The aim of this thesis is to study the effects of reducing retinoic acid (RA) levels in the embryonic face on jaw morphogenesis. One member of the Cytochrome P26 class of enzymes, *CYP26A1*, which degrades retinol products, was locally overexpressed in chicken embryos. I hypothesized that lowering RA levels would either affect jaw patterning, cell survival and/or cytodifferentiation. Chicken embryos at stage 15 and 20 (E2.5, 3.5) were injected with RCAS::*hCYP26A1* in one of three facial prominences, frontonasal mass, maxillary and mandibular prominence. Embryos were fixed 12 days later at stage 39 to examine external and skeletal anatomy. Virus injection into stage 15 and 20 embryos showed similar phenotypes except that embryos injected at stage 15 were more severely affected. Almost all embryos injected at stage 15 had reduced cartilage and bone and some injected in the frontonasal mass and maxillary prominence showed clefts. I next investigated whether endogenous RA levels were reduced by the virus. Wholemount in situ hybridization showed that *RARβ*, a direct target of RA signaling, and *RALDH2*, a RA synthesizing enzyme, were downregulated on the treated side. Expression of indirect targets of RA were also tested but were generally unaffected. The use of a RARE-luciferase reporter showed that the response to exogenous RA was inhibited when *CYP26A1* virus was present, though not by a significant amount. Thus the *RARβ* gene expression and luciferase data suggest the CYP26A1 virus had moderately decreased the levels of RA. The mechanism underlying bone and cartilage differentiation phenotype was examined next. I found that phenotypes could be detected as early as stage 30. There was decreased area of alkaline phosphatase staining and decreased cross sectional area of Meckel's cartilage in treated embryos. Cell proliferation was decreased and apoptosis was increased in the bone condensations, however cellular dynamics were unaffected in Meckel's cartilage. In conclusion, RA is required for expansion of intramembranous bone and cartilage condensations in a stage but not position specific manner.

Preface

This project was conducted with the approval of the UBC Animal Ethics board (#A07-0489). This ethics proposal is renewed annually. The embryos used in this study were from White Leghorn eggs from the University of Alberta. The flock is regularly tested for pathogens and is currently disease-free.

Table of contents

List of tables

List of figures

List of abbreviations

Abbreviation	Definition
ADH	Alcohol dehydrogenase
ALDH	Aldehyde dehydrogenase
An	Angular bone
Ar	Articular bone
BAMBI	BMP and activin membrane-bound inhibitor homolog
BCIP	5-bromo- 4-chloro-3-indolylphosphate
BMP	Bone morphogenic protein
BrdU	Bromodeoxyuridine
CRABP	Cellular retinoic acid-binding protein
CYP26A1	Cytochrome P450, family 26, subfamily A, polypeptide 1
DBD	DNA binding domain
De	Dentary bone
DF1	Chicken embryo fibroblast cell line
DMEM	Dulbecco's modified eagle's medium
DODAC-DOPE	N-N-dioleoyl-N,N-dimethylammonium chloride and 1,2-dioleoyl-sn-glycero-3-phosphoethanolamine
EtOH	Ethanol
FBS	Fetal bovine serum
FGF	Fibroblast growth factor
Fnm	Frontonasal mass
GFP	Green fluorescent protein
GoF	Gain of function
HOX	Homeobox
HPLC	High performance liquid chromatography
Ios	Interorbital septum
J	Jugal bone
KOH	Potassium hydroxide
LBD	Ligand binding domain
LiCl	Lithium chloride
Lnp	Lateral nasal prominence
Lof	Loss of function
Mc	Meckel's cartilage
Md	Mandibular prominence
MEIS	Myeloid ectotropic viral integration site homeobox
MeOH	Methanol

Abbreviation	Definition
MSX	Msh homeobox
Mxb	Maxillary bone
Mxp	Maxillary prominence
NBT	Nitroblue tetrazolium chloride
P	Palatine bone
Pa2	Second pharyngeal arch
PBS	Phosphate buffered saline
PFA	Paraformaldehyde
PITX	Pituitary homeobox
Pmx	Premaxillary bone
Pnc	Prenasal cartilage
Pt	Pterygoid bone
Q	Quadrate bone
Qj	Quadratojugal bone
RA	Retinoic acid
RALDH	Retinaldehyde dehydrogenase
RAR	Retinoic acid receptor
RARE	Retinoic acid response element
RBP	Retinol binding protein
RCASBP-Y	Replication-competent avian sarcoma-leukosis virus long terminal repeat with Splice acceptor
RDH	Retinol dehydrogenases
RT-PCR	Real-time polymerase chain reaction
RXR	Retinoid X receptor
San	Surangular bone
SDR	Short-chain dehydrogenase/reductase
SOX	Sex determining region Y homeobox
Sp	Splenial bone
STRA6	Stimulated by retinoic acid gene 6
TESPA	3-Aminopropyl triethoxysilane
TUNEL	Terminal deoxynucleotide transferase mediated dUTP nick end labeling
VAD	Vitamin A deficient

Acknowledgments

Chapter 1 – Introduction

Retinoids are lipid-soluble vitamins that must be obtained from the diet. One of the main active derivatives is all-*trans*-retinoic acid (RA). The RA molecule is important in regulating an array of developmental processes: anterior posterior patterning via hox gene regulation, neurogenesis, cardiogenesis, body axis extension, limb bud outgrowth, pharyngeal pouch morphogenesis, eye development and early facial morphogenesis (Niederreither and Dolle, 2008).

It is important to have just the right level of RA during development. McCaffery et al (2003) described experiments where mice and quail were systemically exposed to high doses of RA through the diet, resulting in body axis defects, neural defects (McCaffery et al., 2003). Beads soaked with RA can also be transplanted into embryos and these cause either patterning defects such as mirror image duplication of the digits or failure of digits to form (Tickle et al., 1982; Tickle et al., 1985). The same RA beads placed in the limb have dramatic effects on the upper beak causing a complete truncation of outgrowth (Tamarin et al., 1984). Beads placed directly into the face also result in a specific truncation of the centre of the upper beak indicating there is just one region that is especially sensitive to the levels of RA (Richman and Delgado, 1995).

In designing my studies I wanted to focus on the consequences of RA deficiency since this is the more prevalent problem in humans. Retinoic acid deficiency in humans has the highest incidence in Southeast Asia and Africa and affects around one third of all children within

five years of age (Black et al., 2008). The earliest symptom of retinoic acid deficiency is impaired vision in lower light settings. The reason for the vision effects is that retinal functions as a visual chromophore. Annually, between 250,000 to 500,000 children become blind by this mechanism. Inhibition of the retinoic acid signaling pathway due to deficiency in the ligand has been attributed to impaired immune system, hyperkeratosis, enamel hypoplasia in the teeth, as well as cleft palate, among many other defects (Black et al., 2008). Dietary supplementation is a public health measure being implemented in many populations around the globe (Ye et al., 2000).

In my thesis I will be analyzing the role of retinoids in later stages of facial development extending until skeletal differentiation has taken place. I will be using the chicken model in which it is possible to manipulate the embryo and the retinoid pathway directly in the egg. In order to understand my approach, which is to interfere with one of the terminal steps in the RA pathway, I need to first review RA synthesis, transport, transcriptional activity and breakdown.

1.1   Retinoic acid transport, biosynthesis and catabolism

1.1.1 Retinol transport

Retinoic acid precursors enter the body through the diet and are converted into various forms before becoming biologically active. Retinoids (retinyl esters) are taken up by the liver, where they are then hydrolyzed by enzymes into retinol. In this form, retinol can bind to the transport enzyme RBP which is synthesized by the liver. RBP is a protein in the lipocalin family which has a hydrophobic domain where retinol binds. The binding of retinol to RBP protects

retinol from metabolism. In addition to preventing elimination of plasma retinol by the kidney, the RBP-retinol complex associates with transthyretin (TTR) (Zanotti et al., 2004).

In order for retinol to enter tissues, it can either diffuse in directly or can use a cell membrane receptor specifically for RBPs called Stimulated by Retinoic Acid gene 6 (STRA6)(Kawaguchi et al., 2007). *STRA6* is broadly expressed in the embryo thus provides little or no spatiotemporal specificity to the signaling (Kawaguchi et al., 2007; Reijntjes et al., 2010). Tissue-specific enzymes or retinol dehydrogenases (RDH) oxidize and convert retinol into retinaldehyde. RDHs either belong to the alcohol dehydrogenase (ADH) family of enzymes or the short-chain dehydrogenase/reductase (SDR) family. SDR products are likely used in processes other than RA synthesis (Theodosiou et al., 2010) and will not be considered further. There are 4 ADHs of which only Adh1 and 4 are expressed in a tissue specific manner in mice (Theodosiou et al., 2010). Studies have shown that Adh1 and Adh4 are necessary in cases of extreme excess or extreme deficiency of retinoids (Molotkov et al., 2002). However, Adh knockout studies revealed that Adhs have redundant roles in embryo development, thus do not directly contribute to the patterning roles of RA (Deltour et al., 1999).

1.1.2 Retinaldehyde conversion to the active metabolite, retinoic acid

The oxidation of retinol into RA is carried out in multiple steps. First, ADHs oxidize retinol ($C_{20}H_{30}O$) into retinaldehyde ($C_{20}H_{28}O$) (Figure 1) . Next, retinaldehyde dehydrogenases (RALDHs) further oxidize retinaldehyde ($C_{20}H_{28}O$) into all-*trans*-retinoic acid ($C_{20}H_{28}O_2$) (Figure 1). This irreversible process is carried out by the ALDH class of enzymes. There are two classes

of ALDHs, ALDH1A and ALDH8. The ALDH8 class has one member, called ALDH4, while ALDH1A include three members, ALDH1A1 (aka: RALDH1), ALDH1A2 (aka: RALDH2), and ALDH1A3 (aka: RALDH3) which are all present in vertebrates (Theodosiou et al., 2010). *Raldh1, Raldh2*, and *Raldh3* enzymes show spatiotemporally restricted expression patterns in mouse (McCaffery et al., 1999; Niederreither et al., 2002b; Niederreither et al., 1997) and chicken embryo development (Blentic et al., 2003; Suzuki et al., 2000). In situ hybridization showed that *Raldh2* is the first of the family to be expressed at stage 4 in the mesoderm in chicken embryos. This in situ hybridization data is corroborated by HPLC and reporter assays of embryonic mesoderm which showed that RA levels plus activity (shown by reporter assays) correlates with the start of *Raldh2* expression (Niederreither et al., 1997; Niederreither et al., 2002c).

1.1.3 Canonical retinoic acid receptors and transcriptional activity

The synthesized RA can then be transported into the nucleus to activate transcription or transported to a neighboring cell. This transportation of RA is done by binding to cellular RA binding proteins in cytoplasm called CRABP-I and CRABP-II. Tissues sensitive to levels of RA express CRABPs. Evidence suggests that CRABP-II acts as a co-regulator of RA signaling by directly translocating synthesized RA to the nucleus (Theodosiou et al., 2010).

The RA ligand has in the past been called a nuclear hormone since it uses a similar type of multi-domain receptor to those used by estrogens. Retinoic acid enters the nucleus where it binds to retinoid receptors (Figure 1). There are two main domains, the DNA binding domain (DBD) which recognizes specific DNA response elements in promoters of genes, while the ligand binding domain (LBD) binds the RA. In addition the LBD has a region which promotes

dimerization with other RAR or related RXR receptors. The LBD mediates ligand-dependent activation/repression of gene transcription (Theodosiou et al., 2010).

There are two subgroups of retinoid receptors, RA receptors (RARs) and the retinoid X receptors (RXRs). The RARs include RARα, RARβ and RARγ. RARs bind to all-*trans* RA and 9-*cis* RA. Interestingly, RARs that are unliganded can also bind to response elements and repress transcription (Weston et al., 2003). In contrast, RXRs bind to 9-*cis* RA but not all-*trans*-RA. RXRs bind as heterodimers with a variety of receptors including RAR, thyroid hormone receptor, vitamin D receptor, and peroxisome proliferator-activated receptor. It is unclear if RXRs have an active role in transcription in these heterodimers, but studies in RAR/RXR dimers determined that in the absence of a ligand bound to RAR, the activity of RXR is silenced (Theodosiou et al., 2010)

The identification of the RAR response element was made in 1989 by de Thé and colleagues (de Thé et al., 1989). They found that RARβ transcription is directly regulated by RA (de Thé et al., 1989). Various lengths of the RARβ promoter region were fused with luciferase and sv40 polyadenylation signal to detect promoter activity. A 27-base pair retinoic acid response element (RARE) 59 base pairs upstream of the transcriptional start site for RARβ was isolated and shown to induce transcription in the presence of RA. The sequence reads: 5'-GGGTAGG**GTTCAC**CGAAA**GTTCAC**TCG-3'. Note that the sequence contains a perfect repeat of the motif GTTCAC (de Thé et al., 1989) but palindromes are also possible (Balmer and Blomhoff, 2005). It is this small response element that has formed the basis for retinoic acid activity assays in vitro (Wagner et al., 1992) and in vivo (Balkan et al., 1992; Rossant et al., 1991).

1.1.4 RA degradation

RA catabolism is just as important as synthesis in the overall regulation of cellular RA levels. The CYP26 family of enzymes (Cytochrome P 450 class) oxidizes RA into its inactive metabolites (4-hydroxy RA and 4-oxo RA; Fig. 1; (Niederreither et al., 2002a). In general, the three *Cyp26* genes, *Cyp26a1, Cyp26b1* and *Cyp26c1* are expressed in non-overlapping domains, suggesting that they act independently and have different roles in RA catabolism (Theodosiou et al., 2010). Some investigators have shown that the metabolites of CYP26 are active (Reijntjes et al., 2005) however this data is controversial. Using a *RARE-hsp68-lacZ* transgene which should respond to any type of retinoid signaling (Balkan et al., 1992; Rossant et al., 1991), it has been shown that knockout of CYP26A1 results in an upregulation of the reporter, showing that there is an increase of RA signaling in the absence of *CYP26* enzymes. Thus, the phenotypes seen are the result of teratogenic levels of RA signaling, and not from the lack of *CYP26* metabolites. (Niederreither et al., 2002a). However, an avian study has shown using RT-PCR that the "inactive" metabolites of the *CYP26* enzymes: 4-oxo-RA, 4-OH-RA and 5,6-epoxy-RA were able to upregulate *CYP26A1* and *CYP26B1* whereas *CYP26C1* was downregulated (Reijntjes et al., 2005). *RALDH2* which was unaffected by bead implants soaked in RA, was downregulated when beads soaked with 4-oxo-RA, 4-OH-RA and 5,6-epoxy-RA were implanted. These transcriptional activities were shown to be mediated mostly through binding with RARα. The key result supporting activity of the breakdown products of RA was the ability 4-oxo-RA, 4-OH-RA or 5,6-epoxy-RA to rescue the development of RA-deficient quail (Reijntjes et al., 2005). It is not clear why these chicken data are different than the mouse genetic data.

Figure 1.1 Overview of retinoic acid synthesis, entry into the nucleus, transcriptional activity and catabolism
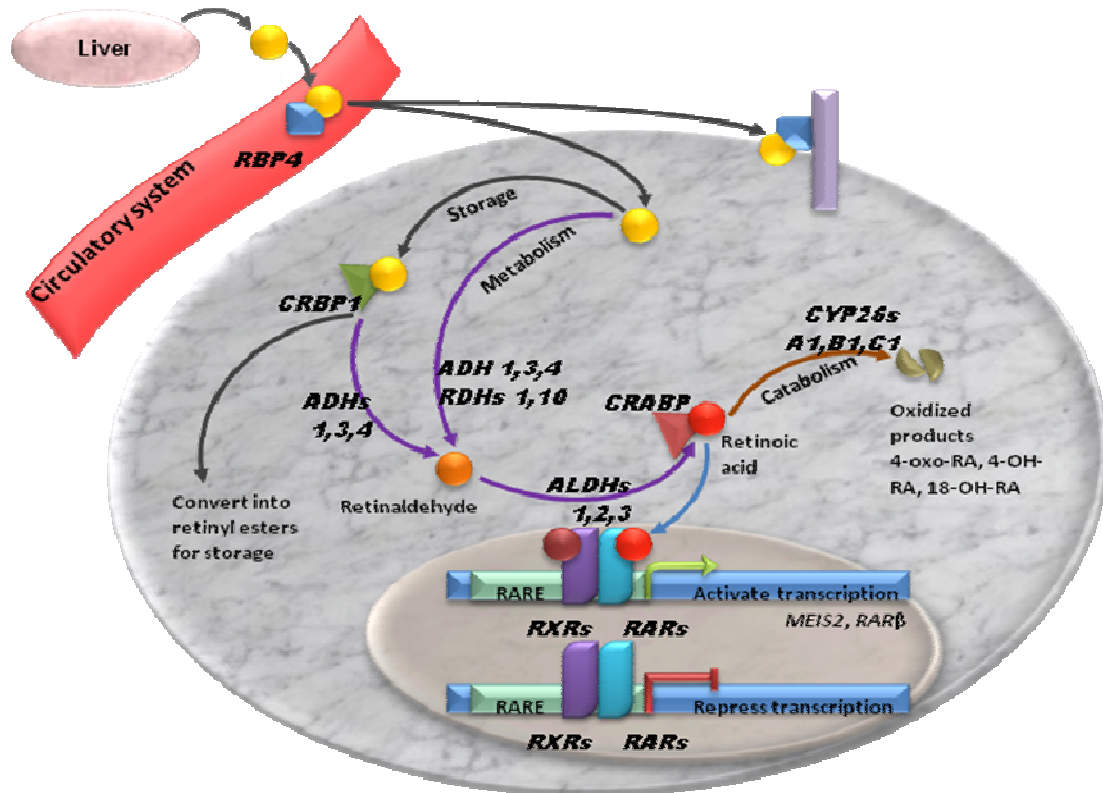
Figure 1.1. Overview of Retinoic acid synthesis, entry into the nucleus, transcriptional activity and catabolism. RBP4 – Retinol binding protein 4, STRA6 - Stimulated by retinoic acid gene 6 homolog, CRBP - Cellular Retinol Binding Protein, ALDH – Aldehyde dehydrogenases, RDH – retinol dehydrogenases, CRABP – Cellular retinoic acid binding protein, CYP26s – Cytochrome P450 family 26.

Table 1.1a Summary of animal models that affect RA levels or transcriptional activity

PART OF PATHWAY TARGETED	GAIN OR LOSS OF FUNCTION	MANIPULATION	RESULTS	REFERENCES
Ligand	LoF	Vitamin A deficient quail	Died at stage 20, uninformative for skeleton	(Quinlan et al., 2002; Wilson et al., 2004)
Synthesizing enzymes	LoF	Antagonists of RALDH enzymes: Citral, DEAB, Disulphram	Citral caused large apoptotic population and huge defect	enzymes (Citral (Schneider et al., 2001; Song et al., 2004), DEAB (Reijntjes et al., 2007)) Disulphram (Stratford et al., 1996)
Synthesizing enzymes	LoF	Genetic deletion of RALDHs with RA supplement for embryo survival	RA supplement to mother rescues embryos from early lethality. Ocular and nasal defects. Neural tube patterning defects	(Dupe et al., 2003; Niederreither et al., 2002d; Wilson et al., 2004)
Nuclear receptors	LoF	Genetic deletion of RARs and RXRs	Embryos early lethal. Defects in the respiratory tract, the heart, thyroid glands, urinary system, digestive tract	(Lohnes et al., 1994; Lufkin et al., 1993; Maden, 2000; Maden, 2006b; Tay et al., 2009)
Nuclear receptors	LoF	Antagonists of RARs and RXRs	Spinal cord patterning defects	(Maden, 2006a)
Ligand	GoF	RA-soaked bead implants	Beads implanted into the nasal pit caused clefts, bead implants into limbs caused duplicated digits and truncated limbs with no digits, bead implants with RA and Noggin transformed the maxillary prominence identity into frontonasal mass	(Lee et al., 2001; Richman and Delgado, 1995; Song et al., 2004; Tamarin et al., 1984; Tickle et al., 1982)
Ligand	GoF	RA supplement in diet; systemic exposure	Abnormalities in cerebellum and hindbrain of mice.	(McCaffery et al., 1999)
Catabolic enzyme	GoF	Genetic deletion of *CYP26*s in mice	Posteriorization of hindbrain, defects in midbrain and forebrain, truncated hind limb buds	(Ribes et al., 2007; Sakai et al., 2004)

Table 1.1b Summary of animal models that affect RA levels or transcriptional activity

PART OF PATHWAY TARGETED	GAIN OR LOSS OF FUNCTION	MANIPULATION	RESULTS	REFERENCES
Catabolic enzyme	GoF	antagonism of *Cyp26* using R115866 in mice	Loss of caudal pharyngeal arches, otic vesicle defects, reduced sizes of all facial prominences, DiGeorge Syndrome-like heart defects	(Roberts et al., 2006; Stoppie et al., 2000)
Synthesizing enzyme	GoF	Manipulation of other genes that leads to ectopic expression of RALDHs	KOs of Crkl+/-;Tbx1+/- lead to upregulation of Raldh2 causing pharyngeal and heart defects.	(Guris et al., 2006)
Catabolic enzyme	LoF	or down-regulation of *CYP26*s	Tbx1 null mice have down regulated *CYP26A1*, *B1*, and *C1*, leading to pharyngeal arch defects, otic vesicle defects, reduced sizes of all facial prominences, and DiGeorge Syndrome-like heart defects	(Roberts et al., 2006)
Synthesizing enzyme	GoF	Direct transgenic overexpression of RALDHs (Raldh1 a1, a2, a3)		Not done by anyone yet
Catabolic enzyme	Lof	Transgenic overexpression of CYP genes		Not done by anyone yet

1.2   The role of endogenous RA in facial development

How much RA is present in the face? Are there regional differences in the level of RA signalling in different parts of the face? We need to review this data in order to design experiments to decrease RA activity. A method of detecting RA levels in vivo is using the RARE-LacZ reporter mice (Balkan et al., 1992; Rossant et al., 1991). These studies showed relatively strong RA activity in the upper face between E9.5 and E10.5 with almost no expression in the first pharyngeal or mandibular arch. This suggests that RA may be either synthesized at higher levels in the upper face or broken down more rapidly in the lower face. Indeed, *RALDH* genes are expressed in specific domains of the upper face. *RALDH2* first appears in the dorsal regions of the eye, the mesenchyme adjacent to the eye whereas *RALDH3* shows is expressed slightly later at stage 20 in the nasal placode and in the mesenchyme ventral of the eyes (Blentic et al., 2003). In the first pharyngeal arch, *RALDH2* is expressed in the dorsal epithelium of the first pharyngeal cleft at stage 18. Thus strong signals of *RALDH* suggest that there is relatively high RA synthesis in the upper face but less so in the lower face.

Alternatively, there may be increased breakdown of RA in the mandibular prominence which would lead to less reporter activity. *Cyp26A1* first appears at E7.75 in the cranial mesoderm of the mouse. This expression quickly disappears however, and shifts to be expressed only in the caudal regions of the embryo from E8.25 onward. From then on, *Cyp26A1* expression in the head is restricted to a weak expression in the mesenchyme of the 1st

pharyngeal cleft (Sakai et al., 2001). *Cyp26B1* is generally not expressed in the face. At E9.5, it is weakly expressed in the ectoderm of the 2nd pharyngeal cleft and in the ectoderm of the developing forelimbs (Sakai et al., 2004). Early in development at E8.0-8.5, *Cyp26C1*is expressed in the mesenchyme of the hindbrain regions corresponding to rhombomeres 2 and 4, in the mandibular prominence epithelium, and in the mesenchyme lateral to the hindbrain (Tahayato et al., 2003). Later on at E9.5, *Cyp26C1* continues to be expressed in rhombomere 2 and the mandibular prominence, and is also expressed in the maxillary prominence epithelium and strongly expressed in the lateral mesenchyme adjacent to the 2nd and 3rd pharyngeal arches. From this point in development onward, *Cyp26C1* expression decreases overall until it is weakly expressed in the lateral pharyngeal mesenchyme at E11.5 (Tahayato et al., 2003).

In the chicken model, *CYP26A1* is strongly expressed as early as stage 6 in the cranial neural plate and the edges of the lateral neural plate, and the caudal end of the Hensen's node. At stage 10, *CYP26A1* is absent from the head and is expressed in the neural ectoderm at rhombomere 3, as well as in the neural tube and the tail bud. From here on, *CYP26B1* and *CYP26C1* are the only homologues present in the head region and are restricted to expression in the rhombomeres. At stage 14, *CYP26C1* is expressed in rhombomeres 2 to 7. At stage 16, *CYP26B1* is expressed in rhombomere 1 and less strongly in rhombomeres 4 and 6 (Reijntjes et al., 2005). This expression data suggests that in the mouse *Cyp26C1* could be responsible for lowering the level of RA activity in the mandibular prominence. The chicken may be different and since no in vivo reporter exists for chicken other methods to assess the level of RA must be used.

The most direct way to quantify RA is to dissect the tissues of interest and use high pressure liquid chromatography (HPLC) to measure the levels of RA. One study from the Maden group did just that. They dissected stage 24 chick embryos and found the frontonasal mass has relatively high levels of RA (Maden et al., 1998). The same study used a second less direct approach. Fragments of stage 24 mandibular prominence tissue were placed on F9 reporter cells that express RARE-LacZ. The levels of LacZ staining are assessed qualitatively in this assay so it is difficult to make precise statements about the quantity of RA. Nonetheless the facial fragments appear to have similar properties to the posterior limb bud which has high levels of RA. LacZ was also induced by stage 15 pharyngeal arch tissue, but at much lower levels. This is in contrast to the mouse reporter data that showed almost no lacZ staining in the first arch and mandibular prominence (Balkan et al., 1992; Rossant et al., 1991). It is possible that when cells from the face are placed into culture the *CYP26* enzymes are less active, allowing more RA to accumulate and thus stimulating the reporter.

The effect of dietary loss of RA on developmental processes has been studied extensively using vitamin A deficient quails and rats (Table 1.1a and 1.1b). In addition various genetic models targeting RA synthesizing enzymes in mice have also been created (Table 1.1a and 1.1b). In these models the importance of endogenous RA in development is highlighted by the early lethality of RA deficiency (Halilagic et al., 2007; Halilagic et al., 2003; Niederreither et al., 1997). However this means that it is difficult to determine the later roles of RA in development. In order to circumvent these problems, the mothers of *Raldh2/3* knockout embryos were artificially supplemented with active retinoic acid to allow normal implantation

and gastrulation (Dupe et al., 2003; Niederreither et al., 2002c; Wilson et al., 2004). Due to early lethality of VAD quail (lethal after 4 days of incubation) we don't know the true function of endogenous RA in patterning and skeletal development.

1.3   Facial prominences and their skeletal derivatives

1.3.1 NCC origins of face

The neural crest cells have several unique properties that set them apart from many other cells in the embryo. First they are migratory, second they undergo epithelial to mesenchymal transformation and third they are multipotent. All neural crest cells originate from the dorsal neural folds and undergo epithelial-mesenchymal transformation before migration. The neural crest cells that contribute to the face are collectively called the cranial neural crest cells. These include all neural crest cells anterior to the otic vesicles (primitive ear). A further subdivision of the cranial neural crest is the facial neural crest. Facial neural crest cells are all those that originate from the prosencephalon, mesencephalon and the anterior hindbrain or rhombomeres 1 and 2 (Creuzet, 2005). All neural crest cells posterior than the hindbrain are called the trunk neural crest cells.

The striking property of neural crest cells is that they are multipotent. Studies using explants with premigratory neural crest cells which were cultured then stained for specific antibodies detected that the neural crest cells can form various cell types such as neurons and glial cells, smooth muscle cells, endocrine cells, and pigment cells (Abzhanov et al., 2003). Cranial neural crest cells unique from trunk neural crest in that they alone can also form cartilage and intramembranous bone. Transplant experiments which inserted quail tissues

containing cranial neural crest cells into chicks have been used for more than 40 years since quail cells can be permanently distinguished from chicken and yet behave similar to chicken cells (Le Douarin, 1969). Such interspecific grafting experiments showed that aside from the occipital and some of the otic tissues which are mesodermally derived, almost all of the head skeleton is cranial neural crest derived (Le Douarin et al., 2004).

The migration of neural crest cells has been extensively studied. They do not randomly disperse into the mesenchyme, rather, they travel in groups and their migration is spatiotemporally specified. The most anterior neural crest cells depart the neural tube first and the wave extends posteriorly. There are gaps in the migrating stream of neural crest cells adjacent to rhomobomeres 3 and 5 (Lumsden et al., 1991).

Cells originating from between the prosencephalon and mesencephalon begin to emigrate from the neural tube at around stage 9 (Tosney, 1982). Groups of cells originating from different levels of the brain emigrate towards distinct regions of the face. Neural crest cells originating from just cranial of the developing eyes emigrate towards the prosencephalon and then ventrally to populate the frontonasal mass. Cells from the mesencephalon emigrate to populate the mesenchyme in the rest of the upper face including the maxillary prominence and distal mandibular prominence. The cells from the anterior hindbrain (1st and 2nd rhombomeres) emigrate and populate the proximal mandibular prominence including the joint (quadrate). The 2nd pharyngeal arch is mostly populated by neural crest cells from the 2nd and 4th rhombomeres (Couly et al., 1998).

The Homeobox (Hox) genes are a group genes related to Antennapedia class genes in Drosophila. They have in common a 180 bp sequence that encodes a homeobox DNA-binding domain. The Hox genes are expressed throughout the anterior-posterior axis of the embryo, but are not expressed anterior to rhombomere 2 (Couly et a. 1998). Thus, all cranial neural crest cells arise from Hox-negative domains while trunk neural crest cells arise from Hox-positive domains (Abzhanov et al., 2003; Creuzet et al., 2002). The Hox-negative cranial neural crest cells have the highest skeletogenic potential. They form the majority of the cartilage and connective tissues in the face and are the only cell type that can form intramembranous bones, which include nearly all of the bones in the face. This is in contrast to the Hox-positive cells which cannot make cartilage or bone except in cell culture with addition of growth factors (Abzhanov et al., 2003).

In early development, as the cranial neural crest cells populate their respective environments, they are regulated by FGFs and BMPs to undergo proliferation and apoptosis, respectively, to shape the facial prominences (Ashique et al., 2002; Francis et al., 1994; Szabo-Rogers et al., 2008). Later on, BMPs regulate genes with contrasting roles to undergo bone and cartilage differentiation. For example, BMPs upregulate *SOX9* which regulates cartilage differentiation (Healy et al., 1999; Hu et al., 2008), and also *MSX1* and *MSX2* which negatively regulate differentiation and promote apoptosis (Ashique et al., 2002; Barlow and Francis-West, 1997; Higashihori et al., 2009; Semba et al., 2000).

1.3.2 The facial prominences

The embryonic face is formed from distinct protrusions called facial prominences. The facial prominences must undergo proliferation and apoptosis to grow larger to contact each other, and then undergo fusion and merging to form a complete face. The main facial prominences involved with the development of the upper and lower beak of the chick are: the frontonasal mass, which forms the midline of the upper beak; the lateral nasal prominence, which forms the sides of the nose; the maxillary prominence, which forms the lateral structures and the palate of the upper beak; and the mandibular prominence (also known as the first pharyngeal arch), which forms all of the elements of the lower jaw. The second pharyngeal arch has a small role in the formation of the lower beak where it contributes to the formation of the tongue.

The mechanisms underlying the identity of the facial prominence have been extensively studied. A study by Richman and Tickle (Richman and Tickle, 1989) described grafting experiments where frontonasal mass, maxillary prominence, and mandibular prominence tissues were grafted onto the wing bud. It was found that it is the mesenchyme, and not the epithelia, of the facial prominences that determine their identity. Grafts of frontonasal mass and mandibular prominence into the wing bud developed cartilage structures. This study supported that the neural crest cells in the mesenchyme determine the identity of the prominence derivatives (Richman and Tickle, 1989). The maxillary prominence which was originally thought to be a portion of the mandibular prominence was later determined by Lee et al (Lee et al., 2004) to be a distinct population of cells that do not integrate with the mandibular prominence. The lateral nasal prominence which is lateral to the frontonasal mass, can also

16

differentiate into bone and cartilage in the form of the nasal bones and the nasal conchae. The ability of this facial prominence to differentiate is regulated by intrinsic mesenchymal abilities as well as epithelial-mesenchymal interactions (MacDonald et al., 2004).

As the facial prominences are populated by cranial neural crest cells, they are multipotent and are able to form intramembranous bone, cartilage, as well as connective tissues. An excellent example of this is the mandibular prominence which is the sole contributor of the lower jaw (Richman and Tickle, 1989; Wedden et al., 1987), and is able to form all of the bone elements as well as Meckel's cartilage, which runs the entire length of the lower jaw (Figure 1.2).

Failure for the facial prominences to contact, fuse or merge results in gaps, or clefts in the face. In humans as with chicks, disconnection between the frontonasal mass and the maxillary prominence result in an upper beak cleft.

Figure 1.2 Fate of the facial prominences
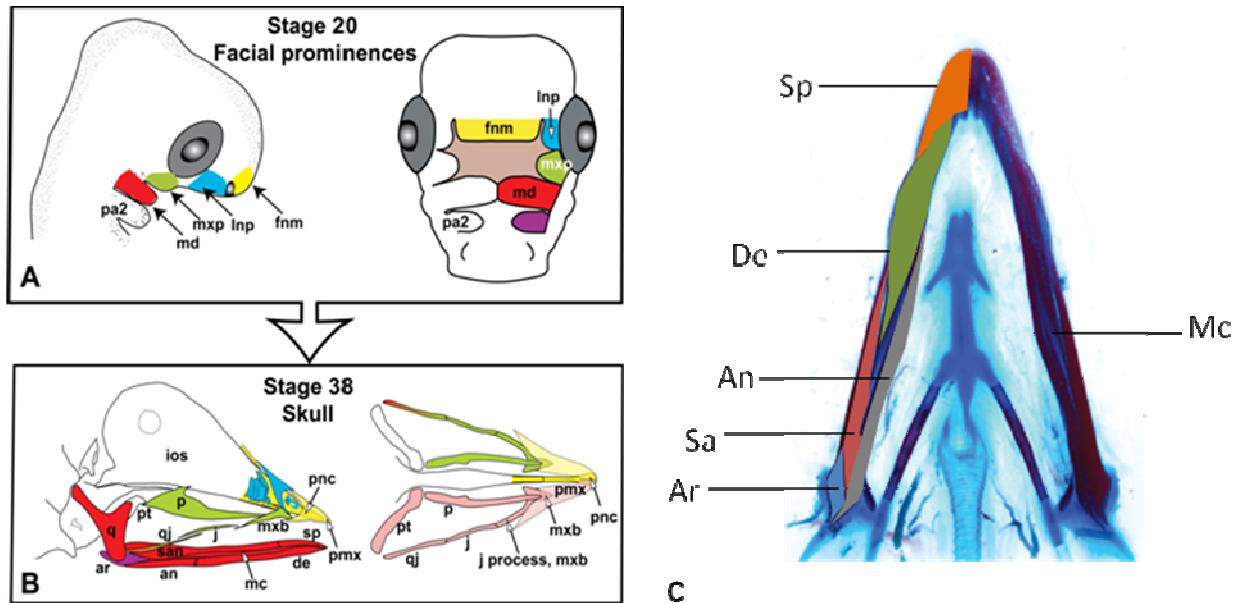
Figure 1.2. The skeletal elements of the face are derived from specific facial prominences. (A) Lateral (left) and frontal (right) views of the chicken embryo face at stage 20. The facial prominences are distinctly identifiable at this stage. The frontonasal mass forms the midline structures of the face. The lateral nasal prominence forms the sides of the nose. The maxillary prominence forms the sides of the upper jaw. The mandibular prominence forms all of the elements of the lower jaw. The second pharyngeal arch contributes minimally to the face, forming parts of the tongue. (B) Lateral (left) and palatal (right) views of the chicken embryo face at stage 38. All bones present in the adult chicken face are well developed. (C) Ventral view of the mandible at stage 38. Meckel's cartilage runs the entire length of the mandible on both sides, surrounded by bone elements. fnm – frontonasal mass, lnp – lateral nasal prominence, mxp – maxillary prominence, md – mandibular prominence, pa2 – second pharyngeal arch, ios – interorbital septum, pnc –prenasal cartilage, pmx – premaxilla, mxb – maxillary bone, p – palatine, j – jugal, qj – quadratojugal, q – quadrate, pt – pterygoid, ar – articular, san – surangular, an – angular, mc – Meckel's cartilage, de – dentary, sp – splenial. (A) and (B) modified from Joy Richman.

1.3.3 Skeletal derivatives of the facial prominences

At stage 39, the chicken embryo beak has formed all of the skeletal elements that will be present post-natally (Table 1.2). At the tip of the upper beak is the premaxilla. Caudal to the tip are processes of the premaxillary bone which extend towards and contacts other bones in the upper beak (Fig. 1.2A,B). There are two nasal processes of the premaxilla that are thin bone structures that extend caudally along the dorsal midline. On either side of the nasal processes are the triangular nasal bones, which contain the cartilaginous nasal conchae. Ventral to the nasal processes are two maxillary processes of the premaxilla which extend distally from the midline to meet the maxillary bones. The maxillary bones have a larger main body which contacts the premaxilla and have a thin process which extends caudally to contact the jugal bones. The jugal bones are a thin bone that bridges the thin processes of the maxillary bones and the quadratojugal bones, which are long bones caudal to the jugal bones. Together, the premaxilla, maxillas, jugal bones and quadratojugal bones extend via processes to contact each other and form the upper beak (Fig. 1.2B).

From the palatal view, these bones form a distinct "V" shape. Easily visible from a palatal view are the pterygoids and the palatine bones (Fig. 1.2B). The pterygoids are connected to the caudal end of the quadratojugal and they extend slightly cranially towards the midline. The palatines are long bones that begin where the pterygoids meet the midline and have a long process that extends to meet the body of the maxillary bones. The pterygoids and palatines are the main bones that form the roof of the chicken oral cavity (Fig. 1.2B).

The upper and lower beak bones are connected via the quadrates, a larger triangular shaped bone at the two proximal corners of the beak (Fig. 1.2A). The lower beak consists of a core of cartilage called Meckel's cartilage that extends from just ventral of the quadrate to meet at the distal tip of the beak. Meckel's cartilage is surrounded by five bones on either side (Fig. 1.2C) : the articular bone is located dorsal of the Meckel's cartilage where it articulates with the quadrate bone or joint. Adjacent to the articular is the surangular bone, more distal from the hinge of the jaw. Across the Meckel's cartilage from the surangular is the more ventral angular bone. The distal half of the lower beak consists of the dentary and splenial bones, dorsal and ventral of the Meckel's cartilage respectively.

Table 1.2 Skeletal derivatives of the facial prominences

Facial prominence		Skeletal derivative			
Fnm	Frontonasal mass	**F**	Frontal bone (not shown in diagram)	intramembranous bone
		Pmx	Premaxilla	intramembranous bone
		Pnc	Prenasal cartilage	cartilage
		IOS	Interorbital septum distal part	cartilage
Lnp	Lateral nasal prominence	**Nb**	Nasal bone	intramembranous bone
		Nc	Nasal conchae	cartilage
Mxp	Maxillary prominence	**Mxb**	Maxillary bone	intramembranous bone
		J	Jugal	intramembranous bone
		P	Palatine	intramembranous bone
		Qj	Quadratojugal	intramembranous bone
Md	Mandibular prominence	**Qj**	Quadratojugal	intramembranous bone
		Q	Quadrate (Endochondral)	intramembranous bone
		Sa	Surangular	intramembranous bone
		An	Angulare	intramembranous bone
		Sp	Splenial	intramembranous bone
		De	Dentary	intramembranous bone
		MC	Meckel's Cartilage	cartilage
PA2	2nd pharyngeal arch	**Tongue**	Tongue (entoglossum)	cartilage

1.4 Rationale

The importance of endogenous RA in development is highlighted by the early lethality of RA deficient models. High levels of endogenous RA in the face, which directly regulates gene expression via its nuclear receptors, and RA deficiencies, such as compound knockouts of RALDHs, show critical roles for RA in facial morphogenesis (Table 1.1a and 1.1b). Due to early lethality of RALDH knockouts (RALDH knockouts are lethal at E9.5-E10.5; (Halilagic et al., 2007; Niederreither et al., 2002c) and VAD quail (lethal after 4 days of incubation; (Halilagic et al., 2003) we don't know the true function of endogenous RA in patterning and skeletal development.

1.5 Approach

My approach is to locally overexpress *hCYP26A1* in chicken embryos to deplete RA in target tissue. Locally overexpressing *hCYP26A1* has advantages over other methods of locally depleting endogenous RA. Chemicals that block RA synthesis by RALDHs (such as DEAB) and antagonize RARs (such as CD2366) are an effective but less elegant approach. They may have many unwanted cytotoxic effects. Locally injecting RNAi against RALDHs is also possible but has may have off target effects which makes interpretation of the results difficult. In contrast, increasing expression of *CYP26A1* via use of an avian specific retrovirus, RCASBP, takes mimics the endogenous degradation process of RA, thereby locally reducing RA with minimal risk of interfering with uninterested developmental mechanisms.

1.6 Hypotheses

1. RA is required for outgrowth of facial prominences

2. RA is required for patterning of the jaws

3. RA is required for skeletal differentiation

4. There are spatial and temporal differences in the requirement for RA

1.7   Objectives

1. To characterize the position-specific requirements of RA signaling following injection into the frontonasal mass, maxillary or mandibular prominences

2. To characterize the stage specific effects.

3. To characterize the mechanism of the *CYP26A1* effects on development of the face and on skeletal differentiation.

Chapter 2 – Methods

2.1 Virus preparation

Human *CYP26A1* was cloned into the Gateway modified avian retrovirus RCASBP-Y (Loftus et al., 2001). The RCASBPA containing GFP was obtained from S. Gaunt (RCAS::*GFP*). Pathogen-free DF1 chicken fibroblast cells (ATCC cat no: CRL-1590) were transfected with RCAS::*hCYP26A1* proviral DNA or with RCAS::*GFP* using the DODAC-DOPE method. Transfections combined 2.74 µg of RCAS::*hCYP26A1* or RCAS::*GFP* DNA with 1 µl of DODAC-DOPE and incubated the mixture at room temperature for 45 minutes. The lipoplexes were then added to a 35 mm dish of 80% confluent DF1 cells cultured in 0.5mL of Complete Media with 10% Fetal Calf Serum. The cells were then incubated at 37°C overnight in a CO_2 incubator. Cell were split the next day, and then split every 3 days thereafter in 100 mm dishes.

After a minimum of 2 weeks post-transfection, the cells were allowed to grow to 70% confluency, before changing the media. Media was collected from 12 plates after 24 hours and stored at 4^oC overnight. New media was added to the cells and collected again after 24 hours then the cells were discarded. Media from both collections were combined and spun them down at 25,000 rpm at 4^oC for 2.5 hours in a Beckman SW28 rotor. Immediately after the centrifuge stopped, the supernatant was discarded and viral pellets was allowed to dry for 10 minutes, then 100uL of Optimem media was slowly added without disrupting the pellet. The tubes with pellets were covered, placed in ice and kept in the cold room overnight. The next morning, the pellets were suspended in Optimem and transferred into 1.5 ml eppendorf tubes. The tubes were quickly spun to separate the cellular debris then the supernatant was separated into aliquots of 10uL which were snap frozen in a dry ice-methanol bath then stored in a -80^oC freezer.

2.2 Embryo injections

Embryos at HH-15 or HH-20 (Hamburger and Hamilton, 1951) were injected using glass needles pulled with at Sutter vertical needle puller. Viral particles were injected using a General Valve Picospritzer microinjector and a Leica micromanipulator. In general 5 pulses were delivered to each stage 15 embryo and 7-10 pulses were delivered to each stage 20 embryo. The frontonasal mass was targeted just proximal of the developing nasal pits (Fig. 2.1 B). The maxillary prominence was targeted by injecting into the mesenchyme caudal and ventral to the optic cup, just above the first pharyngeal cleft (Fig. 2.1 C). The mandibular prominence was targeted by injecting from the dorsal side of the prominence towards the ventral side (Fig. 2.1 D).

Figure 2.1 Sites of embryo injection in a stage 15 chicken embryo
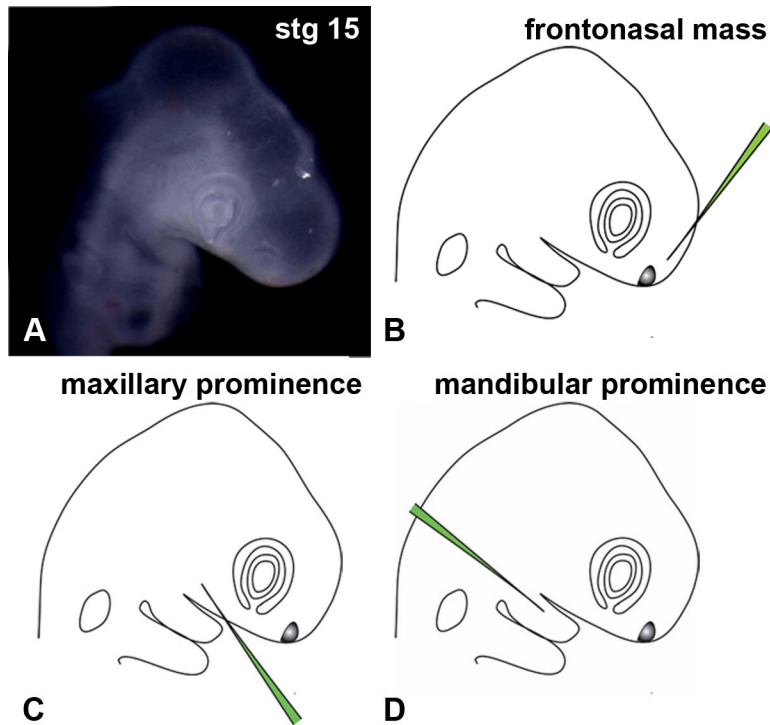
Figure 2.1. Sites of embryo injection in a stage 15 chicken embryo. (A) Lateral view of a stage 15 chicken embryo. (B) Injections in the frontonasal mass were done by inserting the needle from the cranial side, pointing towards just medial of the nasal pits. (C) Injections in the maxillary prominence were done by inserting the needle from the ventral side, pointing into the mesenchyme just behind the eyes. (D) Injections in the mandibular prominence were done by inserting the needle from the proximal end of the mandibular prominence, pointing towards the distal end.

2.3   **Wholemount in-situ hybridization (WISH)**

For all probes synthesized, 1μg of linearized plasmid DNA was used and gel purified with the Qiagen QIAquick Gel Extraction Kit (catalog no. 28704). Klenow fragments (New England Biolabs catalog no. M0212S) were added to templates that had 3' overhangs to prevent the RNA polymerase from binding to this end. RNA antisense probes were synthesized to hybridize with sense RNA in the embryos using dig labeled UTP. The DNA template was removed using RNAse-free DNAse I (New England Biolabs catalog no. M0303s) then precipitated in LiCl and ice cold ethanol overnight at -80°C. Probes were resuspended first in RNAse free water and then diluted in hybridization mix to a final concentration of 50 ng/μl. The probe concentration in the hybridization is 1 μg/ml. The wholemount in situ hybridization protocol used was previously published by our lab (Appendix 1; (Song et al., 2004). All hybridizations were carried out using an Intavis in situ hybridization robot. The 3 day protocol in detail is presented in the Appendix.

2.4   **Immunofluorescence antibody staining**

Embryos collected were first fixed in 4% paraformaldehyde in PBS (PFA) then processed into 70% EtOH. The samples were sent to the UBC pathology lab for processing into wax. Final positioning of embryos in molds was done in the lab using a stereomicroscope.

Paraffin sections were placed on TESPA (3-Aminopropyl triethoxysilane)-coated (Sigma-Aldrich, cat no: 440140) slides. Following dewaxing and rehydration, slides were washed 3x in PBS, then sections were steamed with 0.01M pH 6.0 Citrate buffer at 99°C for 15 minutes horizontally in a vegetable steamer. Slides were rinsed 3x with PBS for 3min each, then blocking serum was applied (blocking serum: 50μL 10% Tween-20, 100μL goat serum, 850 μL 1xPBS) and slides were incubated in a humidified chamber at room temperature for 1hr. Then the blocking serum was removed and primary antibodies were applied. Antibodies used include the mouse 3C2 monoclonal antibody raised to avian viral coat

protein (1:3, Developmental Studies Hybridoma Bank, supernatant made in Richman Lab), mouse monoclonal anti-chicken Col2a1 (1:250, Developmental Studies Hybridoma Bank, ascites), and anti-GFP rabbit polyclonal (1:2000, Synaptic Systems). The primary antibody was incubated in humidified chamber at room temperature for 1hr. The 3C2 antibody was recovered for reuse. Slides were rinsed in PBS and secondary antibody applied. The secondary antibody was either anti-mouse for monoclonal antibodies or anti-rabbit for polyclonal antibodies. Both were tagged with Alexa fluor 488 (1:200, Invitrogen). Secondary antibody was incubated in humidified chamber at room temperature for 30min in the dark. The slides were rinsed in PBS and coverslipped with Prolong Gold with DAPI and antifade (Invitrogen). Sections were viewed under blue, green and red fluorescence illumination with an Olympus microscope. All three channels were photographed so that autofluorescent red blood cells would appear orange in the combined image.

2.5 BrdU, TUNEL staining and analysis

Chicken embryos were labeled with BrdU by injecting 50 µl of 100 mM BrdU into the amniotic sac two hours prior to fixation. Embryos were removed from the egg, fixed in 4% PFA and then processed into wax. The Becton Dickenson BrdU antibody was used in a 1:200 concentration with the same antigen retrieval as described in section 2.6. TUNEL was carried out using the Chemicon Apotag kit (S7111) with digoxygenin labeled dUTP. This kit amplifies the signal with a FITC secondary antibody to digoxygenin.

Quantification of cell proliferation and apoptosis was carried out using the particle counter Plugin for ImageJ. First a mask was created to identify the area to be counted. Then green cells were counted in the green channel to obtain the total number of labeled cells. For BrdU, the total cell number was determined by counting DAPI positive nuclei. The proportion of BrdU positive cells was determined for each section whereas the absolute number of TUNEL positive cells was used.

2.6 Micromass cultures – luciferase activity

In order to obtain mesenchyme that was expressing *CYP26A1* or *GFP* it was necessary to perform a two stage experiment. Embryos were injected first at stage 10 with RCAS::*CYP26A1* or RCAS::GFP to infect the mandibular prominence bilaterally. These embryos were incubated a further 72h to reach stage 24 and the only mandibular prominences were dissected. Mandibular prominences were dissected into ice-cold sterile Hank's solution (Hank's solution: 10%-FBS, 10%-10x Hank's w/o Ca^{++} and Mg^{++}, sterile ddH$_2$O). To remove ectoderm from the mesenchyme serum containing media was removed and replaced with 2% crude Trypsin, made in Hank's w/o Ca^{++} and Mg^{++}. Tissues were incubated at 4°C for 1.5hrs in a 35 mm culture dish. The tissues were then transferred into Hank's solution with serum and kept cold on an ice slab during epithelial stripping. The remaining mesenchymal cores were transferred into 2mL Eppendorf tubes and were topped off to 500 μl with Hank's solution containing serum. The tissue cells were mechanically dissociated by vigorous pipetting, then pelleted by centrifuge for 5 minutes at 6500rpm at 4°C. Hank's solution was removed and 1mL (depending on pellet size) of Hank's solution was used to resuspend the pellet. A hemocytometer was used to count the cells. Cell were pelleted again and were resuspended in Micromass Media at a concentration of 2x10^7 cells/mL. Micromass media consisted of: 5 mL-FBS, 26 mL-F12, 17 mL-DMEM, 500 μL-Antibiotics, 500uL-Glutamine, 50 μL-Ascorbic acid, 500 μL-βGlycerol Phosphate. At this point transfection mixture containing the RARE-Luciferase reporter plasmid and the Renilla transfection control plasmid was added to the cell suspension. For each 100 uL of 2x10^7 cells/mL of cell suspension, 5 μg of total plasmids was transfected. Within the 5 μg of DNA, 9 parts were composed of RARE-Luciferase and 1 part was Renilla-luciferase. The 9:1 Renilla/Luciferase plasmid mixture was incubated for with DODAC-DOPE lipids in the ratio of 2.74 ug plasmid: 1 μl lipid. A 10 μl droplet of the cell suspension was plated on the culture dish to form a single micromass culture and 4-5 spots were plated in each 35 mm dish. To allow the cells to attach to the plate, the spots were incubated at 37°C for a minimum of 1hr before the dish was flooded

with 1 ml of Micromass Media. In some cultures 30 nM all-*trans*-retinoic acid or DMSO was added to the micromass culture media after 1 day of culture. The spots were cultured for an additional 48 hours, making the total culture period 72h.

2.7 Luciferase assay

The Promega Dual Luciferase Assay kit was used as per manufacturer's directions (cat no. E1910). Following 72h of growth, the cultures were lysed in a passive lysis buffer and then stored until analysis in the -80 freezer. Luciferase luminescence was detected in triplicate (3 technical replicates) and a minimum of 3 spots per treatment (biological replicate) using the Lmax Microplate Luminometer (Underhill lab).

2.8 Alkaline phosphatase staining of sections

Embryos were dissected out in ice-cold PBS at HH stages 30 and 32 and processed into 4% PFA at $4^{o}C$ overnight. The specimens were then washed with PBS twice then processed into paraffin and sectioned at 7 µm thickness in the frontal plane. Sections were dewaxed and rehydrated with a xylene and alcohol series. To detect alkaline phosphatase activity, the substrate, nitroblue tetrazolium chloride/ 5-bromo- 4-chloro-3-indolylphosphate (NBT/BCIP) detection solution is applied directly to sections and stopped after alkaline phosphatase positive condensations were visible (after approximately 30 min to 1 hr). The sections were then counterstained with 0.5% Methyl Green in 0.1 M Sodium Acetate, air dried and coverslipped with Entallen.

The cross sectional area of cartilage and bone was measured from photographs of sections using Image J.

2.9 Skeletal staining for skulls and limbs

Skulls and limbs were collected from E12 or stage 37 embryos. The eyes and skin of skulls were dissected out before processing while limbs were left intact. Protocols as published in Song et al., 2004

were used. Briefly, embryos were fixed in 100%EtOH followed by Acetone for 4 days each. Acetone was washed off with dH_2O. Alcian Blue and Alizarin Red stain was made fresh (Stain: 1vol. 0.3% Alcian blue 8GX in 70% EtOH, 1 vol 0.1% Alizarin red S in 95% EtOH, 1 vol Acetic acid, 17vol 70%EtOH). The samples were stained at room temperature on a shaker for 10 days. The stain was then rinsed off with dH_2O before clearing in 2%KOH in H_2O for a few hours then changed into 2%KOH+20%glycerol. The clearing solution was changed every other day. When cleared, the samples were put into 50% glycerol then 100% glycerol. Embryos were photographed fresh in PBS and then again after staining and clearing using a Sony 850 SLR camera with a macrolens. To visualize the skeleton, substage illumination was used.

Chapter 3 – Results

3.1 Temporal and spatial effects of *CYP26A1* overexpression on beak development

Retroviral infections were performed in three regions of the face, the frontonasal mass, maxillary prominence and mandibular prominence and delivered the virus at either stage 15 or stage 20. There injections were designed to test whether there were temporal or spatially specific responses to the increased expression of *CYP26A1*. The total number of embryos treated is summarized in Table 3.1.

3.1.1 Correct targeting of the virus to individual facial prominences

In order to localize the virus to different parts of the beak it was necessary to inject the tissues of origin accurately. A preliminary set of experiments was therefore carried out with RCAS::GFP to determine whether the frontonasal mass, maxillary and mandibular prominences were successfully targeted. 3C2 antibody staining of virus injected embryos showed that the injections were well localized with very few viral particles dispersed to the untreated side (Fig. 3.1A-C).

Table 3.1 Number of specimens collected for this study

Stage of embryo	Part of face targeted	Embryos collected for skulls	Embryos for in situ hybridization	Number of embryos for BrdU and TUNEL		
			Stage of embryo at end of experiment			
		Stage 38	Stage 24	Stage 24	Stage 30	Stage 32
Stage 15	Fnm	18	64	7	0	0
	Mxp	21	420	7	0	0
	Md	20	28	2	2	5
		Stage of embryo at end of experiment				
		Stage 38	Stage 28			
Stage 20	Fnm	5	17			
	Mxp	7	-			
	Md	6	-			

Figure 3.1 Demonstration that targeting of facial prominences is successful and that the majority of the virus remains unilateral
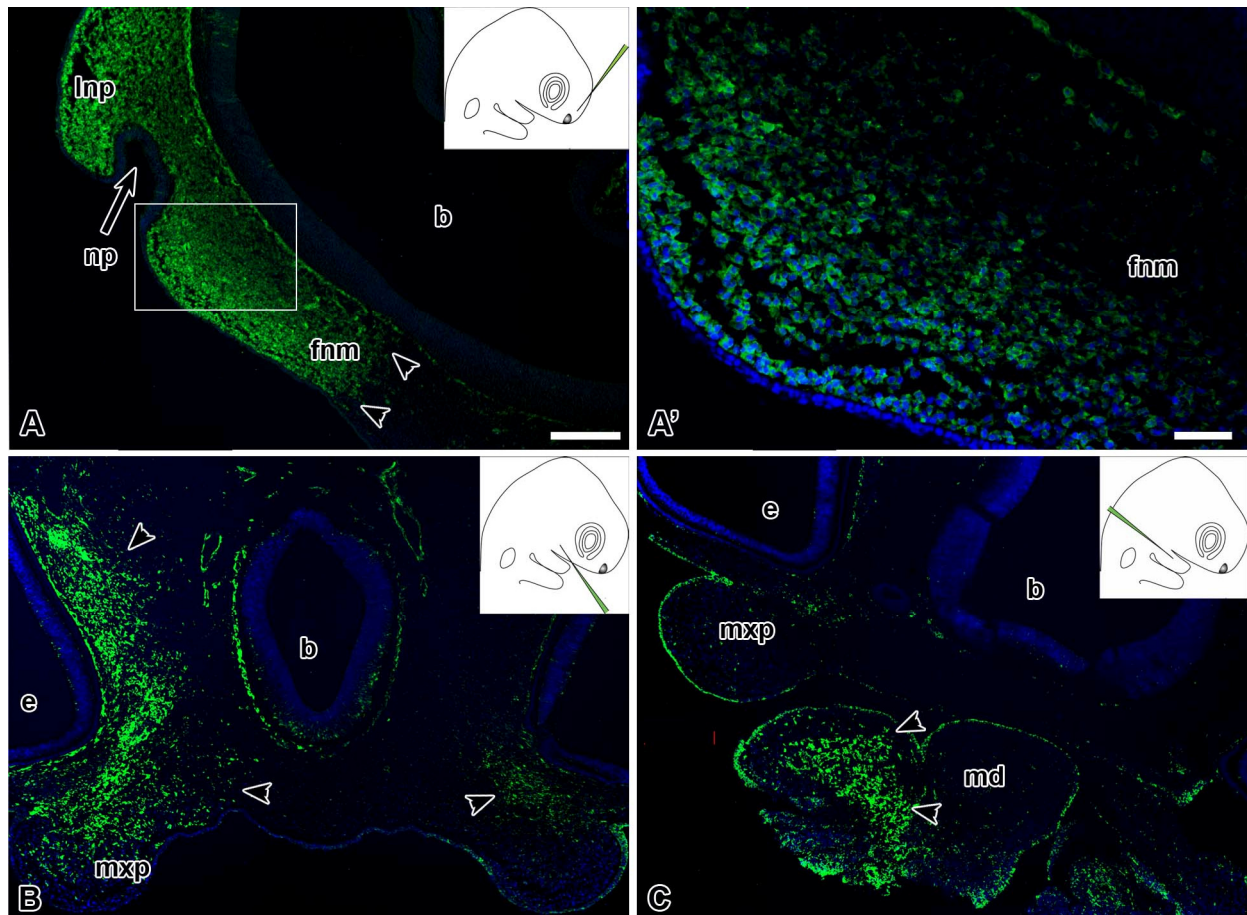
Figure 3.1. Sections of the face stained with the 3C2 antibody detected that the virus was well localized in the injection sites and that the majority of the virus remained unilateral. (A) Injection in the frontonasal mass also infected the lateral nasal prominence. Arrowheads indicate the edge of the virus infected area. Very little virus had spread to the other. (A') higher magnification of the same section in (A). (B) Injection in the maxillary prominence remained on the treated side for the most part. Some virus spread dorsally behind the eye and a few particles had spread to the untreated side. (C) Injection into the mandibular prominence infected cell on the treated side and did not spread to the contralateral side.

Scale bar in (A) indicates 200µm and also applies to (B) and (C). Scale bar in (A') indicates 50µm.

Figure 3.2 Demonstration that virus targets the skeletal elements of the beak in a site specific manner.
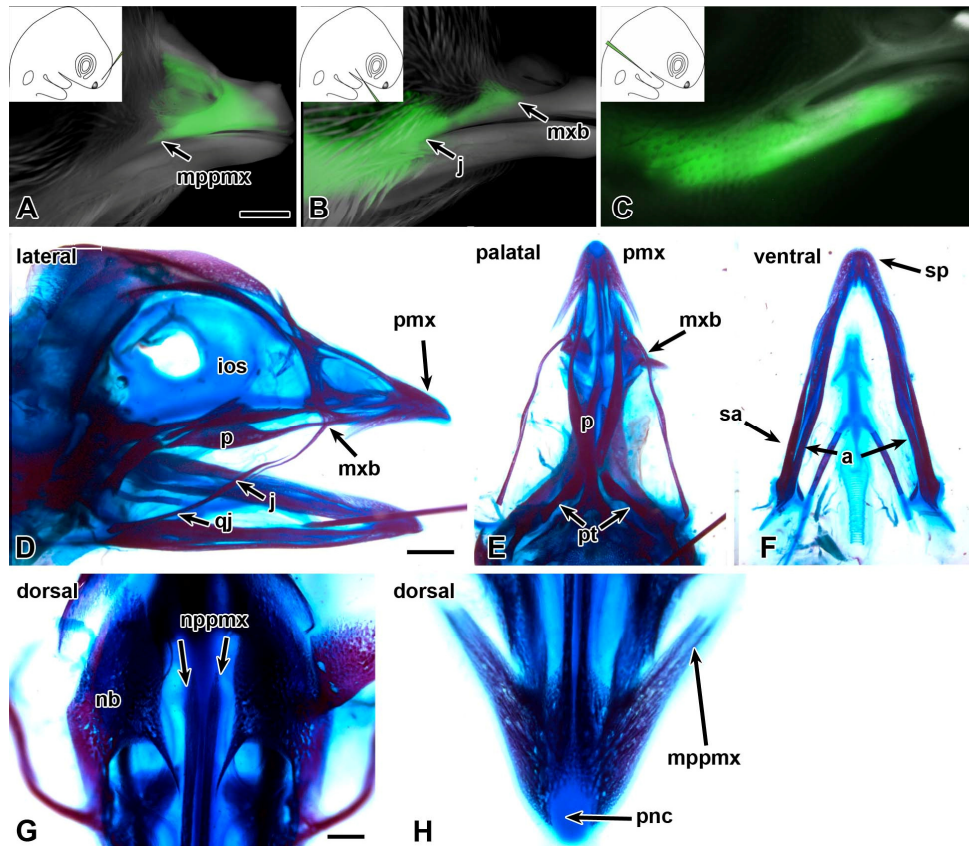
Figure 3.2. GFP virus injected embryos at around stage 38 showed that the virus targeted in the facial prominences only infected the skeletal elements derived from that prominence. Lateral views of GFP virus injected embryos indicate that injection into the frontonasal mass infected the nasal conchae and the premaxilla including the maxillary process of the premaxilla. (B) Injection into the maxillary prominence infected the maxillary bone, the jugal, and other maxillary prominence-derived bones. (C) Injection into the mandibular prominence infected the entire lower jaw on the treated side. (D) Lateral view, (E) palatal view, (F) ventral view of the mandible, (G) high power magnification of the nasal bones from a dorsal view, and (H) high power magnification of the premaxilla from the dorsal view of a stage 39 embryo skull.

Scale bar in (A) indicates 2mm and also applies to (B) and (C). Scale bar in (D) indicates 2mm and also applies to (E) and (F). Scale bar in (G) indicates 0.5mm and also applies to (H).

mppmx – maxillary process of the premaxilla, j – jugal, mxb – maxillary bone, ios – interorbital septum, pmx – premaxilla, p – palatine, qj – quadratojugal, pt – pterygoid, sp – plenial, sa – surangular, a – angular, nppmx – nasal process of the premaxilla, nb – nasal bone, pnc – prenasal cartilage.

3.1.2 Frontonasal mass injections affect upper beak development

The frontonasal mass gives rise to the midline skeletal elements of the upper beak as well as the egg tooth. The GFP injected embryos provide further support for the fate maps already published. When allowed to develop to stage 38, the GFP control embryos had bright fluorescence overlapping the premaxillary bone (Fig.3.2A,D, and H). The virus did not spread into the maxillary bones despite the fact that the globular processes or corners of the frontonasal mass fuse with the maxillary prominences at stage 29. Failure of fusion leads to a separation of the premaxillary and maxillary bones (Szabo-Rogers et al., 2008; Szabo-Rogers et al., 2009). I injected embryos in the frontonasal mass at two different stages of development in order to see whether there were effects on the length or width of the upper beak, deviations and whether clefts were induced. Additionally, we cleared the specimens to examine effects on the skeleton.

Of the embryos injected the majority (n = 13/18, Table 3.2) had an external phenotype (Fig. 3.3A-A'''). The range of phenotypes included embryos with clefts (n = 9), shortened upper beak (n = 10), as well as beak deviations to the left or the right side (n = 13). However when the skulls were cleared nearly all the embryos had skeletal phenotypes (n = 16/18, Table 3.2). RCAS::*hCYP26A1* virus in the frontonasal mass resulted in defects in all of the frontonasal mass and lateral nasal prominence-derived bones. The frontal bone was reduced in size (n = 15) on the treated side. The nasal bone was similarly reduced in size (n = 16). Embryos with the severe nasal bone phenotype often also had a cleft phenotype which is defined as a gap between the premaxillary and maxillary bones (n = 9). The gap was caused by a shortened maxillary process of the premaxilla (n = 15, Fig. 3.2A'',A''') combined with a shorter maxillary bone (n = 12). The right palatine bone (maxillary process) was also much shorter (n = 8) and the jugal bones were occasionally shorter (n = 5). These bones are derivatives of the maxillary prominence and were likely secondarily affected by frontonasal mass injections after lack of fusion of

the facial processes. It is not a direct result of the virus infecting the maxillary prominence as GFP injections into the frontonasal mass showed that injections specifically targeted only the frontonasal mass derivatives (Fig. 3.1A). Unrelated to the cleft there were other effects on skeletal elements such as a shortening of the nasal process of the premaxillary bone (n = 16, Fig. 3.3A'''). In contrast to the membranous bones, the cartilaginous nasal conchae, nasal septum and prenasal cartilage were not affected. Rather, the nasal conchae were not contained in the nasal cavity in those embryos that also had large clefts (n = 10, Fig. 3.3A''. A'''). This was likely a secondary phenotype that occurred as a result of reduced bone structures around the nasal conchae. No phenotype was observed in the mandibular prominence-derived structures.

3.1.2 Maxillary prominence injections cause clefting and palate defects

The maxillary prominence forms the skeletal elements in the upper beak lateral to the midline of the face, and contributes to lip formation by contacting and fusing with the globular process of the frontonasal mass. I injected RCAS::*CYP26A1* or RCAS::*GFP* into the maxillary prominence of embryos at two different stages of development to study the effects on the length of the upper beak, whether deviations and clefts are induced.

Similar to the frontonasal mass injected embryos, around half of the embryos injected into the maxillary prominence exhibited external phenotypes including beak deviations to the left or right side (n = 12/21) and shortening of the beak in embryos with clefts (Fig. 3.3B). When the skull were cleared for further analysis, it was revealed that even more embryos had skeletal phenotypes (n=15/21, Table 3.2). Injection of RCAS::*hCYP26A1* into the maxillary prominence resulted in severe reduction in bone elements derived from the maxillary prominence as well as minor defects in elements from the frontonasal mass. The maxillary bone was shorter and thinner in a majority of embryos (Fig. 3.3B'-B''')

including those that did not have an external phenotype (n = 15). In embryos that had a cleft, the maxillary bone was displaced caudally (Fig. 3.3B'-B'''). The jugal bone was affected in all embryos showing a phenotype and had similar defects as the maxillary bone where they were shorter and thinner (n = 15). The quadratojugal was less often affected, and was also shorter and thinner (n = 8, Fig. 3.3B'')). The palatine bone was also affected in most of the embryos. The phenotypes of the palatine bone ranged from thinner and shorter maxillary process to the entire bone being thinner and shorter (n = 11, Fig. 3.3B'''). The phenotype seen in the maxillary, palatine and jugal bones in maxillary prominence injected embryos differed distinctly from the phenotype seen in frontonasal mass injected embryos where the palatine bones were sometimes shorter, but not thinner (compare Fig. 3.3A'' to B'').

The frontonasal mass-derived elements were also affected in the maxillary prominence injections. However, the phenotypes were much less severe overall than compared to when the frontonasal mass was targeted by the virus. The maxillary process of the premaxilla was shorter in many embryos (n=8, Fig. 3.3B''). As a result of the reduced bone structures around the nose, the nasal conchae were not contained in one of the specimens (Fig. 3.3B'').

Mandibular prominence-derived structures were also affected in one of the specimens. The surangular and quadrate bones were thinner and the Meckel's cartilage was shorter on the treated side (n = 1). It is possible that the virus had spread into the proximal end of the mandibular prominence from the maxillary prominence during injection, thus affecting the bones located near the hinge connecting the upper and lower jaws.

3.1.3 Mandibular prominence injections shorten the lower beak

The GFP virus injected into the mandibular prominence confirms the contributions to the lower jaw and joint (Fig. 3.2C). The mandibular prominence gives rise to all skeletal elements in the lower beak Fig. 3.2F). We injected embryos in the mandibular prominence at two different stages of development in

37

order to see whether there were effects on the length of the lower beak, deviations and failure to form any of the skeletal elements therein.

Nearly all of the embryos injected with RCAS::*hCYP26A1* into the mandibular prominence showed an external phenotype consisting of a deviation of the lower beak towards the right (n = 19/20, Table 3.2, Fig. 3.3C). None of the upper beak bone structures were affected except the quadratojugal, with cellular contributions from maxillary and mandibular prominences, which was thinner in the majority of the embryos (n = 14, Fig. 3.3C'). No clefts were seen in any of the specimens. The surangular and angular bones, the most proximal structures in the mandible, were smaller and thinner in nearly all of the specimens (n = 19, n = 20 respectively, Fig. 3.3C', C''). The dentary and splenial bones were also reduced in size in the majority of the embryos (n = 14, n = 13, respectively, Fig. 3.3C'''). The quadrate was reduced in size in a few embryos (n = 5). Meckel's cartilage, the only cartilage that seems to have been affected by the virus, was thinner and shorter in most of the embryos (n=15, Fig. 3.3C'', C'''). Some cartilaginous elements of the tongue were slightly smaller but this was seen only in a few specimens (n = 3).

Overall, we did not see any spatially restricted susceptibility to *CYP26A1* virus. All regions of the face infected at stage 15 led to beak defects in older embryos. The external appearance is consistent with an inhibition of outgrowth of the facial prominences at an earlier stage which has led to a loss of skeletal elements.

Figure 3.3 Beak phenotypes produced by injection of CYP26A1 virus into different regions of the face
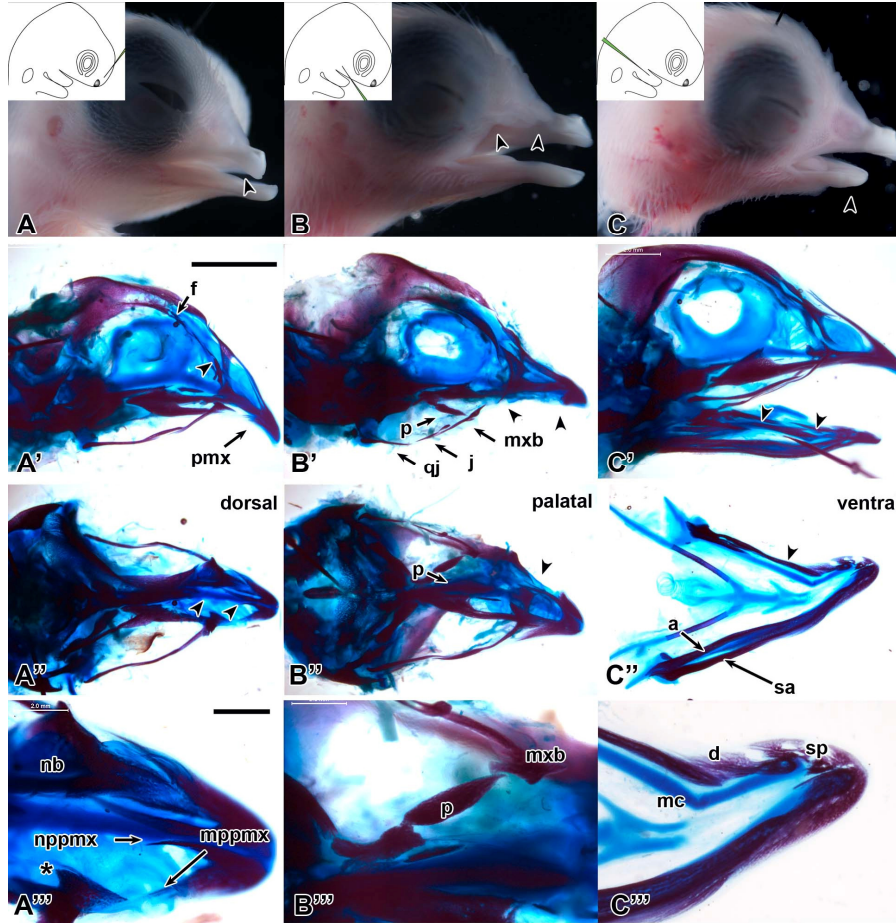
Figure 3.3. Beak phenotypes produced by injection of CYP26A1 virus into different facial prominences. (A) Frontonasal mass injected embryo displayed a shortened upper beak which was also deviated to the right. (A') Skeletal analysis showed that the frontal bone was severely reduced and was almost missing the nasal bone was also missing. The maxillary process of the premaxilla was also reduced. (A'') Dorsal view. The maxillary and mandibular elements were unaffected. (A''') A higher magnification of the dorsal view of the nasal bones and premaxilla. (B') Skeletal analysis showed that the maxillary elements were severely reduced. (B'') Palatal view of the same embryo clearly displayed the reduced palatine bone and the cleft. (B''') A magnified palatal view clearly showing the reduced palatine bone and maxillary bone. (C) Mandibular prominence injected embryos displayed a shortened lower beak. (C') Skeletal analysis showed that all mandibular elements were reduced in size including Meckel's cartilage. (C'') Ventral view of the mandible. (C''') Magnified ventral view of the splenial and dentary bones show that they were reduced in the treated side. Meckel's cartilage was thinner and bent. Scale bar in (A') represents 5mm and applies also to (B'), (C') and (A'')-(C''). Scale bar in (A''') represents 1mm and applies also to (B''') and (C'''). Key: f – frontal bone, pmx – premaxilla, p – palatine, mxb – maxillary bone, j – jugal, qj – quadratojugal, a – angular, sa – surangular, nppmx – nasal process of the premaxilla, nb – nasal bone, mppmx – maxillary process of the premaxilla, sp – plenial, d – dentary, mc – Meckel's cartilage

3.1.4 Stage 20 embryos are less sensitive to the effects of *CYP26A1*

Embryos injected at stage 20 had less severe phenotypes overall (Table 3.3). Therefore by the time the virus was expressed (approximately 24h post injection or stage 24) the mesenchyme was much less susceptible to the effects of RCAS::*CYP26A1*. Only 1 of the frontonasal mass and mandibular injected specimens had a phenotype. In maxillary injected specimens there were more embryos with a phenotype but the changes in bone size and shape were very slight. This suggests there is some stage specificity in the sensitivity to this virus.

Table 3.2 Summary of phenotypes produced by RCAS::hCYP26A1 injected at stage 15

RCAS::*hCYP26A1* injected at stage 15		FNM (n=18)		MXP (n=21)		MD (n=20)	
		n	% affected	n	%	n	% affected
External	**Norm**	5	28%	9	43%	1	5%
	Deviation	13	72%	12	57%	19	95%
	Cleft	9	50%	6	29%	0	0%
FNM derived	**F**	15	83%	5	24%	0	0%
	Nb	16	89%	4	19%	1	5%
	Pmx	15	83%	8	38%	0	0%
	Nc	10	56%	1	5%	0	0%
MXP derived	**Mxb**	12	67%	15	71%	0	0%
	P	8	44%	11	52%	0	0%
	J	5	28%	15	71%	0	0%
	Qj	1	6%	8	38%	15	75%
MD derived	**Sp**	0	0%	0	0%	13	65%
	De	0	0%	0	0%	14	70%
	Sa	0	0%	1	5%	19	95%
	An	0	0%	0	0%	20	100%
	Q	0	0%	1	5%	5	25%
	MC	0	0%	0	0%	3	15%
PA2 derived	**Tongue**	0	0%	0	0%	3	15%

Table 3.3 Summary of phenotypes produced by RCAS::*hCYP26A1* injected at stage 20

RCAS::*hCYP26A1* injected at stage 20		FNM (n=5)		MXP (n=7)		MD (n=6)	
		n	% affected	n	% affected	n	% affected
External	**Norm**	4	80%	6	86%	6	100%
	Deviation	1	20%	1	14%	0	0%
	Cleft	0	0%	0	0%	0	0%
FNM derived	**F**	0	0%	0	0%	0	0%
	Nb	1	20%	1	14%	0	0%
	Pmx	1	20%	0	0%	0	0%
	Nc	0	0%	0	0%	0	0%
MXP derived	**Mxb**	0	0%	1	14%	0	0%
	P	0	0%	2	29%	0	0%
	J	0	0%	5	71%	0	0%
	Qj	0	0%	1	14%	0	0%
MD derived	**Sp**	0	0%	0	0%	0	0%
	De	0	0%	0	0%	0	0%
	Sa	0	0%	0	0%	2	33%
	An	0	0%	0	0%	1	17%
	Q	0	0%	0	0%	0	0%
	MC	0	0%	0	0%	1	17%
PA2 derived	**Tongue**	0	0%	0	0%	1	17%

3.2 CYP26A1 decreases RARE activity

I previously injected *RCAS::hCYP26A1* viral particles into the facial prominences and analyzed the skulls of stage 39 embryos. I found that the virus caused reduced bone and cartilage elements as well as clefts in around half of the embryos injected in the frontonasal mass and the maxillary prominence. It is not clear at this point, however, whether these phenotypes were the result of the specific degradation of RA by *CYP26A1* and whether genes in the RA signalling pathway have been affected. Therefore, I designed an in vitro experiment with an RA activity reporter construct (obtained from the Underhill lab) to measure the RA activity in the facial prominence mesenchyme with or without the *CYP26A1* virus. Furthermore I examined the effects of *CYP26A1* on expression of several known RA target genes using wholemount in situ hybridization.

3.2.1 Luciferase assays show a trend to a decrease in RA activity in the presence of RCAS::*CYP26*

I wanted to measure the level of RA activity in facial mesenchyme in which the CYP26A1 virus was expressed. However to do this in vivo is difficult. Therefore I used the in vitro micromass culture system. In this way I could maintain the cellular context of the RA signalling pathway. I harvested primary mesenchyme cells directly out of the chicken face and placed them into high density cultures. I focused on mandibular mesenchyme since this cell population makes both bone and cartilage in culture (Richman and Crosby, 1990; Wedden et al., 1986) and both tissues were affected in CYP26A1 virus infected embryos. To measure the level of RA activity I used a well-characterized RA response element (RARE) derived from the RAR beta nuclear receptor (de Thé et al., 1989; Rossant et al., 1991). The RARE is driving the luciferase enzyme and thus it is possible to measure the level of luciferase activity in a luminometer. As there is always a delay in the onset of viral expression I injected donor embryos at

stage 10 with the *CYP26A1* or *GFP* control virus, reincubated the embryos for 72h until they reached stage 24 and then dissected the infected mandibular prominences. The mesenchyme was therefore already expressing high levels of the virus at the start of the culture period.

A preliminary luciferase experiment showed that endogenous RA activities of facial mesenchyme in vitro as detected by the RARE-luciferase reporter were low (data not shown). Therefore, in order to better detect changes in RA activity, I challenged the cultures with 30nM of RA in the media on the second day of culture then collected the cultures for luciferase assay after an additional 24 hours. Therefore the cells were grown for a total of 3 days.

Cultures infected with *RCAS::GFP* and cultured in media with DMSO control had low activity (Table 3.4, Fig. 3.4A) . With the addition of 30nM RA, the luciferase activity significantly increased by 5.3-fold (Fig. 3.4A). This shows that all the necessary co-factors are present in chicken mandibular mesenchyme cells for the reporter to function properly. Cultures with no additional RA infected with *RCAS::hCYP261* had low luciferase activity not significantly different than the *RCAS::eGFP* infected cultures (Table 3.4, Fig. 3.4A). With the addition of 30nM of RA in the culture media, however, the luciferase activity only increased by 3.6-fold (Fig. 3.4A). I next performed a 1-way ANOVA test followed by TUKEY's post-hoc test (Statistica v6) to compare groups. I found that the addition of 30nM of RA was able to significantly increase the luciferase reporter activity in both the GFP and CYP infected cultures compared to DMSO control media (Table 3.4, Fig. 3.4A). However, when comparing GFP to CYP infected cultures challenged with 30nM of RA, the decrease in luciferase activity is not statistically significant (Table 3.4).

Table 3.4 Post-hoc testing on luciferase data

	DMSO-GFP	30nM GFP RA	DMSO-CYP	30nM CYP RA
Tukey HSD test; variable Ave Luciferase (Spreadsheet1) **Probabilities for Post Hoc Tests** **Error: Between MS = .07448, df = 8.0000**				
MEAN ± SD	0.312 ±0.159	1.654 ± 0.428	0.316000±0.146	1.206500±0.261
DMSO-GFP		0.001577	0.999998	0.016476
30nM GFP RA	0.001577		0.001604	0.261345
DMSO-CYP	0.999998	0.001604		0.016861
30nM CYP RA	0.016476	0.261345	0.016861	

Figure 3.4 Luciferase data and expression of RARβ suggests that RA signalling is decreased while RALHD2 expression indicates a possible alteration in the level of CYP metabolites

Figure 3.4. Luciferase data and expression of RARβ suggest that RA signalling is decreased while RALDH2 expression indicates a possible alteration in the level of CYP metabolites. (A) Micromass cultures of GFP or CYP infected mandible were challenged with 30nM of RA. There is a trend that RARE activity is reduced in the CYP infected cultures in comparison with the GFP controls. (B) Wholemount in situ using the POL probe shows that the virus is localized in the targeted maxillary prominence. (C) Frontal view of embryo injected with CYP in the maxillary prominence showing that RALDH2 is reduced on the treated side. (C') Lateral view of the right side of the same embryo showing decreased RALDH2 expression in the maxillary prominence. (C'') Lateral view of the untreated side. (D) Frontal view of an embryo injected in the maxillary prominence with CYP virus showing slightly decreased RARβ expression in the maxillary prominence. (D') Lateral view of the right side of the same embryo showing the decreased expression. (D'') Lateral view of the untreated side. Scale bar represents 500µm. Fnm – frontonasal mass, mxp – maxillary prominence, md – mandibular prominence, mmc – maxillomandibular cleft.

The luciferase data shows a trend to a reduction of RA signaling in the luciferase assays however this difference did not reach significance. This is possibly due to the RA concentration being so high that it overwhelmed the promoter. Perhaps lower RA levels would show a significant difference.

3.2.2 Expression of RA target genes is decreased in CYP26A1-treated embryos

In the next experiment an attempt was made to modify the endogenous levels of RA enough to see an effect on downstream target genes. Ten genes were selected that have been shown to be downstream of RA signalling (Table 3.5). RCAS::*CYP26A1* was injected into the maxillary prominence for these studies based primarily on the gene expression pattern for the genes. All of the 10 genes examined were expressed in the maxillary prominence whereas not all are found in the mandibular prominence. From external examination, no changes in size in the maxillary prominence were seen at stage 24 in any of the embryos, thus there was no early growth deficit. This means we can exclude the possibility of decreased gene expression being due to reduced size of facial prominences.

Table 3.5 Summary of gene expression changes in the maxillary prominence of RCAS::CYP26A1 injected embryos

Gene	Increased	Decreased	Unchanged
RALDH2 *N = 7*	0	4	3
RARβ *N = 6*	0	2	4
MEIS2 *N = 4*	1	0	3
BAMBI *N = 4*	0	0	4
PITX2 *N = 4*	0	0	4
FGF8 *N = 5*	0	0	5
MSX1 *N = 9*	0	0	9
MSX2 *N = 4*	0	1	3
BMP4 *N = 4*	0	0	4
BMP7 *N = 4*	0	0	4

3.2.2.1 *RALDH2*

In the chicken at stage 18, *RALDH2* transcripts are found dorsal to the eye but nowhere else in the face (Blentic et al., 2003). These authors did not however examine expression in older embryos. I found that in control embryos injected with RCAS::*GFP, RALDH2* had two very restricted domains of expression, one in the anterior maxillary prominence and the second in the maxillo-mandibular cleft (data not shown but see untreated side in Fig. 3.4C,C'). In contrast, some embryos injected with RCAS::*hCYP261* had noticeably reduced expression on the treated side (Table 3.5, n = 4/7, Fig. 3.4C'). The other three specimens were unaffected by the virus. Some of this variation is likely due to the pattern of viral spread in each embryo.

3.2.2.2 *RARβ*

RARβ is a nuclear receptor which contains a RARE in its promoter. Thus, *RARβ* unlike, RALDH2 is directly regulated by RA. The normal expression pattern of *RARB* had been described (Rowe et al., 1991; Rowe et al., 1992; Song et al., 2004). The main regions with strong expression at stage 24 include the lateral nasal prominences and anterior maxillary prominence. As predicted, *RCAS::hCYP26A1* into the maxillary prominence resulted in a minority of specimens with decreased expression on the injected side (n = 2/6, Fig. 3.4D-D''). The remaining specimens showed even expression on both sides of the face. This data is suggestive of an effect on the RA pathway but further replication is necessary to confirm this result.

3.2.2.3 *Other targets of RA pathway are unaffected by RCAS::CYP26A1*

We analyzed 8 additional genes that have been shown to be regulated by RA although not necessarily through direct interaction with a RARE. We examined the expression of two BMPs that are downstream of RA signalling, *BMP4* and *BMP7* (Rodriguez-Leon et al., 1999). Neither gene was obviously affected, although viral targeting is very reliable in this region (Table 3.5). Next we looked at *BAMBI* which is a decoy BMP receptor and is strongly induced by RA even in the presence of cycloheximide

(Higashihori et al., 2008). Again no change in expression was observed (Fig. 3.5C). We examined the expression of 4 transcription factors *MSX2, MSX1* (Brown et al., 1993), *PITX2* (Kumar and Duester, 2011; Wasiak and Lohnes, 1999) and *MEIS2* (Mercader et al., 2000). All of these also had unchanged patterns of expression on the treated side. Finally since *FGF8* had been shown by us (Song et al., 2004) and others (Maden et al., 2007) to require RA for its expression we also examined this gene carefully. Again no expression changes were induced and no changes in the size of facial prominences were observed.

Thus based on the luciferase, *RALDH2* and *RARβ* data it appears that RA pathway is being disrupted by CYP26A1 however not all targets of RA are affected by the virus. Other approaches are needed to confirm these results. The most sensitive and specific method is Q-RT PCR. Through the use of gene specific primer and probe sequences it is possible to measure levels of gene expression relative to a house keeping gene. This is currently the best way to accurately measure expression differences.

Figure 3.5 Expression of a set of RA target genes is unchanged following CYP26A1 infection of the maxillary prominence
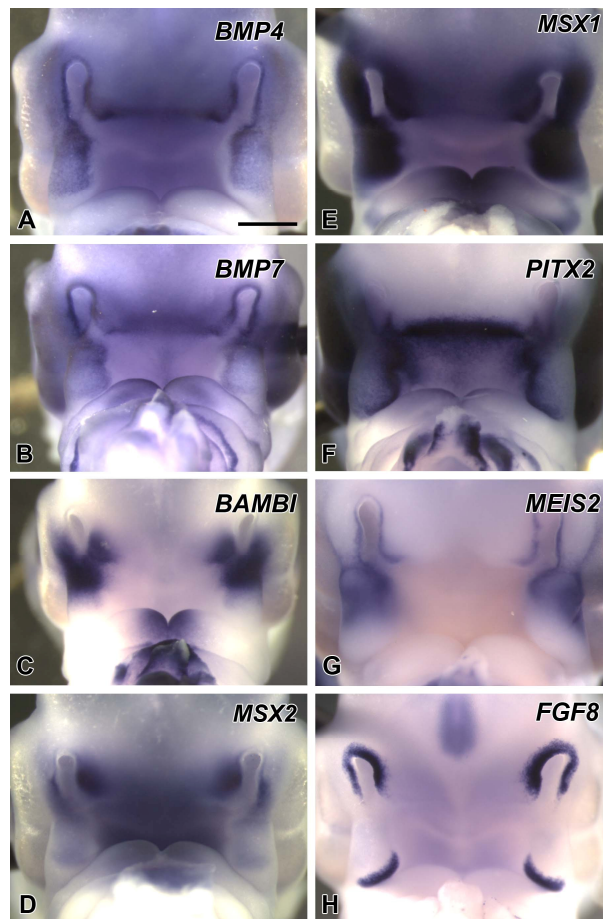
Figure 3.5. Expression of a set of RA target genes is unchanged at stage 24 following CYP26A1 infection of the maxillary prominence at stage 15. *BMP4* (A) and *BMP7* (A) are growth factors that are indirect targets of RA signaling and have a role in inducing bone and cartilage differentiation. (C) *BAMBI* is a membrane bound receptor protein that negatively regulates *TGFβ* signaling. *MSX2* (D), *MSX1* (E), *PITX2* (F), and *MEIS2* (G) are transcription factors that have roles in the patterning of the face. *FGF8* (H) is an embryonic epithelial factor that has been shown in other studies to be downregulated when RA signaling is inhibited. Scale bar represents 500μm.

3.3 Mechanism underlying bone and cartilage differentiation phenotype

The skull phenotypes suggested several possible points in the skeletogenic pathway were affected. First there might be a delay or block in differentiation. Secondly, there could be a selective decrease in proliferation or increase in apoptosis at an earlier stage which either prevented outgrowth or decreased the number of progenitor cells that would go on to form cartilage and bone. Deficiencies in early facial prominences were not seen, thus later stages were studied for mechanism, when differences between the treated and untreated side were present. Mandibular injections were the focus for these studies since I could analyze the effects on both cartilage and bone. The earliest skeletal element to appear in the mandible is Meckel's cartilage at 4.5 days of incubation or stage 24 (Matovinovic and Richman, 1997). Intramembranous bone ossification starts much later. The articular, angular, surangular, dentary, and sphenoid bones initiate at E7-8 or stages 31-33 (Murray, 1963; Romanoff, 1960). Thus, embryos were collected at stage 30 and 32, after cartilage has formed but just when mesenchymal cells are specified to form bone.

3.3.1 Alkaline phosphatase staining shows a reduction in the size of the intramembranous bones but no delay in differentiation.

Alkaline phosphatase activity was used as a marker for early bone formation (Richany et al., 1959; Zernik et al., 1990) and type II collagen or Col2a1 as a marker of cartilage differentiation in order to test the hypothesis that *CYP26A1* delayed or inhibited differentiation of bone and cartilage. Endogenous alkaline phosphatase activity is well preserved in paraformaldehyde, paraffin embedded tissues. Alternate sections in the same embryos were also stained with 3C2 antibody in order to determine where the virus was in relation to bone and cartilage elements.

In the embryos analyzed, the majority of the antibody detection is found in the treated side of the mandible, however because some viral particles entered the blood vessels during injection, the antibody also detected infections in other parts of the head (data not shown). However, the virus is distinctly in higher amounts around the site of injection and is absent in the cartilages and bones (Fig. 3.6C-D').

Alkaline phosphatase activity at stage 30 was detected around Meckel's cartilage in generally a large field corresponding to the angular and surangular bones which are adjacent to each other. At stage 32, the two distinct fields of the angular and surangular bones can be identified, one ventral and one lateral to the cartilage(Fig. 3.6A-B'', Fig. 3.8A,B,E,F). The cartilage did not display any alkaline phosphatase activity. The areas of cartilage and bones were quantified using Image J software. To normalize the data and to compensate for slight differences in development between embryos, the ratios of the bone and cartilage areas were calculated between the treated and untreated sides. I analyzed the following numbers of embryos: stage 30 - 1 GFP and 2 CYP26A1 injected embryos; stage 32 - 2 GFP and 2 CYP26A1 embryos. Three sections per embryo were measured and the mean values used. Since there is only 1 identifiable bone condensation field at stage 30, that area was measured for results. At stage 32 however, two bone condensation fields were identified, thus the sum of their areas

on each side was used in the results. The average ratios of the right versus left side for both cartilage and bone at stage 30 and 32 were always close to 1 for the control GFP injected embryos (Fig. 3.6G, H) . This means the areas of bone and cartilage on the right treated side were generally the same as the left untreated side. At stage 30, there was a significant decrease in the size of meckel's cartilage, despite having a large variation in the severity of the decrease. The bone condensation area, however, was less affected. Although there was a trend of a decrease in bone area, the difference was not significant (Fig. 3.6 G). At stage 32, Meckel's cartilage was decreased in size as with at stage 30. There was less variation in the severity of the reduced size and the reduction was significant. Unlike at stage 30, the bone condensation areas were significantly reduced at stage 32. Taken together, meckel's cartilage and intramembranous bones were both reduced by the CYP26A1 virus but this was more evident at stage 32 (Fig. 3.6B-B'', H) than at stage 30 (Fig. 3.6G). Therefore the *CYP26A1* virus was able to significantly reduce the size of the bone, as defined by alkaline phosphatase staining in the mandible. Interestingly the staining of the bone is just as intense as on the untreated side so there appears to be no delay in differentiation. Thus the skeletal phenotype is visible by stage 30.

Viral infection was confirmed to had taken place within the cartilages and bones using anti viral antibodies (Fig. 3.6C,C'). The left side was uninfected (Fig. 3.6C')The *CYP26A1* virus in this specimen was confined to the right, treated side of the embryo and had expanded to the bone and cartilage (Fig. 3.6D,D').

The expression of Col2a1 was also analyzed in the cartilage since it was possible that the *CYP26A1* virus might have affected matrix quality. Similar to the Alkaline Phosphatase results, there was no difference in the intensity of type II collagen staining. Thus from the preliminary analyses there is a reduction in size of the skeletal elements that may be due to an earlier effect on cell proliferation or apoptosis.

Figure 3.6 Sizes of intramembranous bones and cartilage are reduced at stage 30 and 32 by CYP26A1 virus
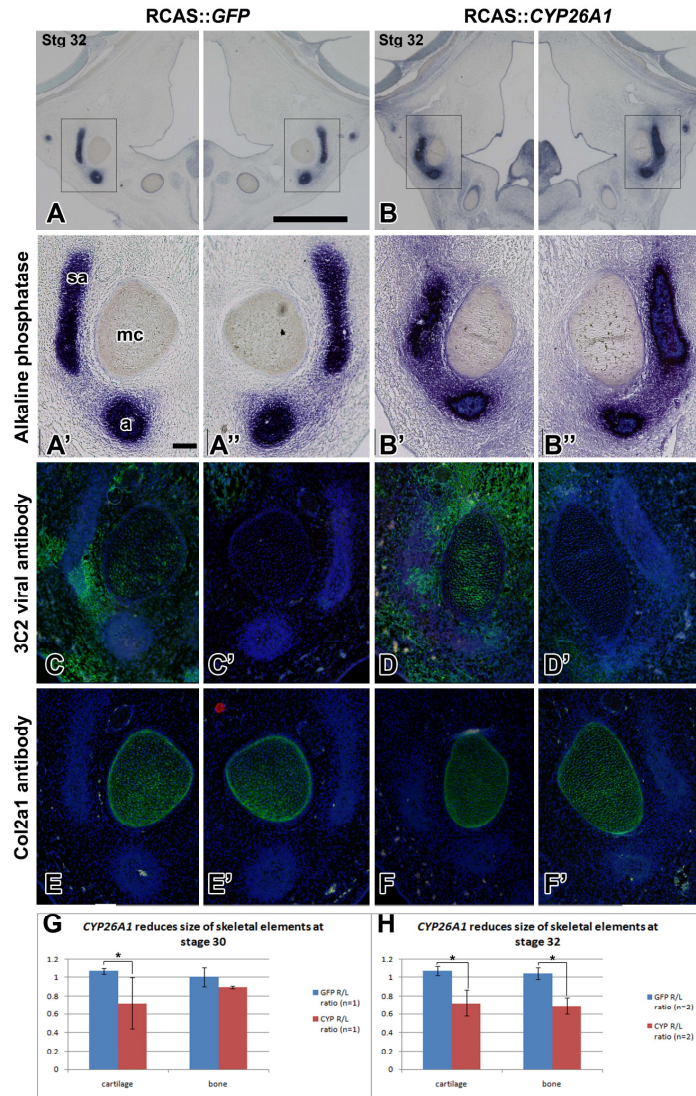
Figure 3.6. Differentiation of intramembranous bone and cartilage is inhibited by CYP26A1 virus. (A) and (B) are sections through stage 32 embryos injected with GFP or CYP26A1 in the mandible, respectively. (A') and (A'') show the treated and untreated sides of a GFP control embryo detected for alkaline phosphatase activity which marks osteogenic cells. It clearly shows the angular and surangular bones which are just beginning to develop. In an embryo injected with CYP26A1 in the mandibular prominence (B') and (B''), the size of the bones and Meckel's cartilage is reduced on the treated side. Dashed lines indicate areas measured in Image J. Viral particles were detected with the 3C2 antibody (C, C', D, D') to verify that the virus had infected the osteogenic cells as well as Meckel's cartilage. Collagen 2 antibody staining (E, E', F, F') showed that there was no difference in expression in Meckel's cartilage in CYP26A1 infected embryos. Measurements of the areas of bone and cartilage at stage 30 (G) revealed that there is a significant decrease in the size of Meckel's cartilage but not the surangular and angular bones in CYP26A1 infected embryos. In stage 32 embryos (H) the differences were more marked. CYP26A1 virus significantly decreased the size of cartilages and bones ($P < 0.05$). Scale bars represent 1 mm in A,B, 50 µm in A'-F'. Key: mc – Meckel's cartilage, sa – surangular, a – angular.

3.3.2 BrdU proliferation is reduced in cartilage but not bone in *CYP26A1*-infected embryos

Cellular mechanisms were investigated next after a delay in differentiation was ruled out. BrdU labeling was analyzed in a single specimen for stage 30 and stage 32 for CYP26A1 and the GFP virus. 2 technical replicates for the CYP26A1 specimen and 1 technical replicate for the GFP specimen. They are the same embryos as used for the Alkaline Phosphatase staining. Meckel's cartilage and the angular bone, as a representative membranous bone, were the focus for the proliferation study (Fig. 3.7A-D). Due to very high cell density in the bone condensations, sections were analyzed at 20X magnification (Fig. 3.7A'-D'). Since viral antibody staining showed that there is little virus on the left side of the head in these specimens (Fig. 3.6C-D'), it is valid to use the left side as an internal control.

The preliminary analysis of the stage 30 embryo shows that there is similar proliferation in the cartilage and bone and that in general right and left sides are almost equivalent (Table 3.6, except of Meckel's cartilage in the *CYP26A1* treated embryo). At stage 32, the impression is that the *CYP26A1* infected embryo has a higher number of BrdU positive cells than the *GFP* infected embryo (compare (Fig. 3.7A,B to C,D) however this is most likely due to variation in the BrdU uptake by the embryo. Staining differences can also occur but will be averaged by analyzing the technical replicates (different sections). With these points in mind, there are still some clear results coming from the stage 32 data. First, the cartilage is reaching maturity and has relatively low proliferation where as osteogenic mesenchyme continues to have a similar frequency of proliferation to its stage 30 counterpart (Table 3.6, Fig. 3.7A-D). Secondly there is generally good agreement between the right and left sides for the cartilage in both the *CYP26A1* and *GFP* infected embryos (Fig. 3.7A-D, Table 3.6). There is also similar proliferation between *CYP26A1* and *GFP* treated embryos suggesting that there is no effect on cartilage. In contrast, there is a

reduction in the proportion of proliferating cells in the angular bone on the right side of *CYP26A1* infected embryo (Fig. 3.7C') as compared to the left, non-infected side (Fig. 3.7D'). These data are suggestive of a repressive effect of the virus specifically on the membranous bones.

Figure 3.7 Cell proliferation was unaffected by CYP26A1 virus at stage 32 however apoptosis was selectively increased in the intramembranous bones
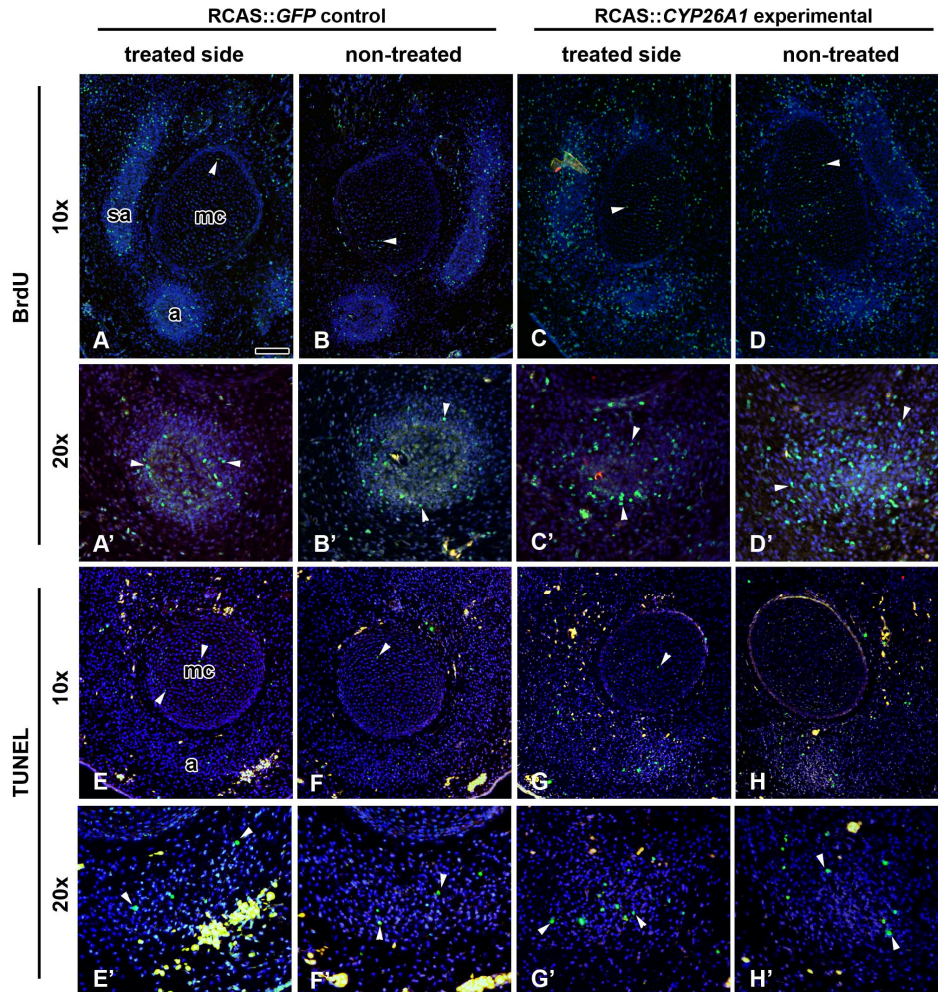
Figure 3.7. Cell proliferation was unaffected by CYP26A1 virus however apoptosis was selectively increased in the intramembranous bones. (A) and (B) show BrdU labeling around Meckel's cartilage of the treated and untreated sides of a control embryo. (A') and (B') are higher magnifications of the angular bone in the same section. (C) and (D) show BrdU labeling in an embryo injected with CYP26A1 virus in the mandibular prominence. Cell proliferation Meckel's cartilage is unchanged between the left and right side. Higher magnification of the angular bone (C') and (D') reveal that there are less cells in the bone condensation in the treated side but the ratio of proliferating cells between the treated and untreated sides remain unchanged. (E) and (F) show TUNEL positive cells in a GFP control embryo. Higher magnification of the angular bone cell condensations (E') and (F') show that the number of TUNEL positive cells are similar between the two sides. (G)

Figure 3.8 Cell apoptosis was increased by CYP26A1 in Meckel's cartilage at stage 30 but unaffected in bone condensations
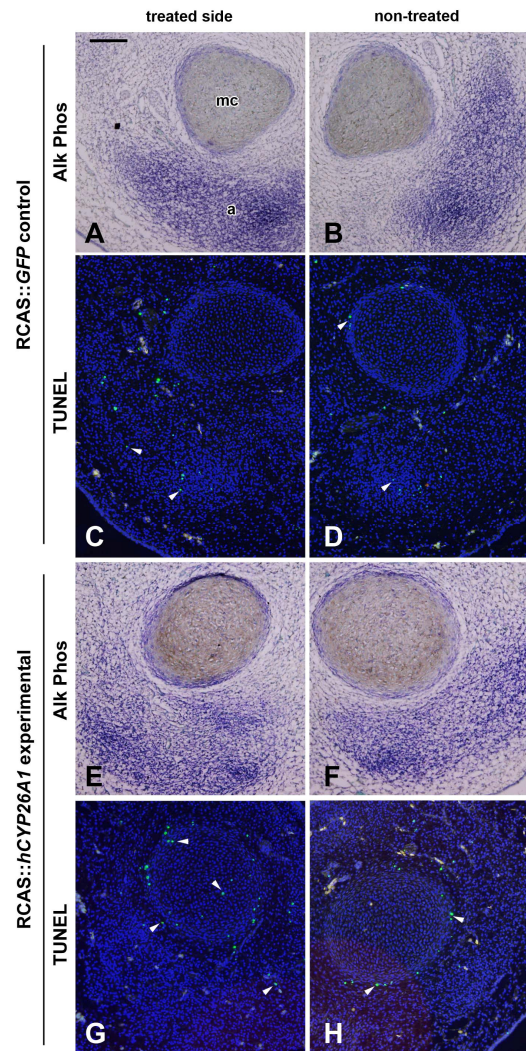
Figure 3.8. Cell apoptosis was increased by CYP26A1 in Meckel's cartilage at stage 30 but unaffected in bone condensations. (A) and (B) show alkaline phosphatase staining of *GFP* injected embryos. (C) and (D) show TUNEL positive cells in the same *GFP* injected embryo. (E) and (F) show alkaline phosphatase staining of *CYP* injected embryo. (G) and (H) show TUNEL positive cells in the same *CYP* injected embryo. Note in (G) and (H) that on the untreated side, TUNEL positive cells were only found around the periphery of Meckel's cartilage while on the treated side, TUNEL positive cells were found around the periphery as well as the middle of the cartilage. There are zero TUNEL positive cells in the angular bone on both sides of the section (G, H). Scale bar = 100 μm. KEY: a – angular, mc – Meckel's cartilage.

Table 3.6 Quantification of BrdU positive cells in GFP or CYP26A1 infected embryos at stage 30 and 32

Stage	Specimen	Tissue	Dapi +tive	BrdU +tive	Percent BrdU
stg 30	GFP1448 L	MC	1025	159	15.51%
stg 30	GFP1448 R	MC	1412	172	12.18%
stg 30	CYP1441 L	MC	881	77	8.74%
stg 30	CYP1441 R	MC	438	67	15.30%
stg 30	GFP1448 L	bone	354	58	16.38%
stg 30	GFP1448 R	bone	412	71	17.23%
stg 30	CYP1441 L	bone	609	92	15.11%
stg 30	CYP1441 R	bone	634	91	14.35%
stg 32	GFP1449 L	MC	632	41	6.49%
stg 32	GFP1449 R	MC	516	44	8.53%
stg 32	CYP1442 L	MC	879	58	6.60%
stg 32	CYP1442 R	MC	688	39	5.67%
stg 32	GFP1449 L	bone	523	78	14.91%
stg 32	GFP1449 R	bone	452	50	11.06%
stg 32	CYP1442 L	bone	321[1]	84.5[1]	26.32%
stg 32	CYP1442 R	bone	390.5[1]	62.5[1]	16.01%

3.3.3 TUNEL positive cells are increased in bone condensations but not in the cartilage in *CYP26A1*-infected mandibles

In the skeletal analysis bone and cartilage elements at stage 30 and 32 were reduced in size in the CYP26A1 injected embryos (Fig. 3.6). The TUNEL assay was carried out in order to determine whether this reduction in size was the result of an increase in apoptosis, resulting in less cells contributing to the condensations.

Stage 32 embryos were first analyzed for apoptosis in Meckel's cartilage and bone condensations as this was the stage at which bone condensations could be easily identified by alkaline phosphatase staining. At stage 32 in Meckel's cartilage, there was no obvious difference in the number of TUNEL positive cells in GFP controls versus *CYP26A1* infected embryos. Most of the sections had less than 5 positive cells in the cartilage (Table 3.7, Fig. 3.7E-H). The angular bone was also analyzed for apoptosis. In contrast to Meckel's cartilage, the sections analyzed had between 10 and 20 positive cells per bone condensation when infected with RCAS::CYP26A1 (Table 3.7, Fig. 3.7E'-H'). It is not clear why the non-treated side of the *CYP26A1* has higher apoptosis than the GFP control but the most likely explanation is inter-embryo variability. Nevertheless the trend is that more sections from treated embryos had higher numbers of TUNEL positive cells.

At stage 30, unlike stage 32, there was an increase in the number of embryos with 10+ TUNEL positive cells in Meckel's cartilage in *CYP26A1* virus injected embryos. 3.8Interestingly, , there was an overall increase in apoptosis on both sides of the mandible. On the untreated side, most embryos had less than 5 TUNEL positive cells in cartilage, however, one embryo had 5-10 TUNEL positive cells and one had 10-15 TUNEL positive cells. This may possibly be due to viral spread to the untreated side. In contrast, on the treated side, a single embryo had less than 5 TUNEL positive cells in Meckel's cartilage, while two embryos had 5-10 TUNEL positive cells and two had 10-20 TUNEL positive cells. Thus the

CYP26A1 virus had increased the number of embryos with higher levels of apoptosis in Meckel's cartilage which could have contributed to the reduction in size.

In the bone condensations at stage 30, the CYP26A1 virus did not appear to affect the level of apoptosis. On the treated and untreated side of CYP virus injected embryos, almost all of the embryos had less than 5 TUNEL positive cells in the bone condensations (Fig. 38G,H). Only one embryo had 5-10 TUNEL positive cells. In GFP injected embryos, all embryos had less than 10 TUNEL positive cells on both sides of the face (Table 3.7, Figure3.8C,D).

From the TUNEL assay at stage 30 and 32, it appears that *CYP26A1* has a stage specific effect on cell survival of cartilage and intramembranous bone formation. *CYP26A1* seems to increase apoptosis in Meckel's cartilage earlier in development up to stage 30, resulting in a decrease in size of cartilage but apoptosis is no longer occurring at stage 32. . In contrast, *CYP26A1* does not seem to affect cell survival of intramembranous bone condensations in earlier stages of development, such as at stage 30. It is only at stage 32 that the effect on apoptosis of *CYP26A1* can first be detected. Taken together, the smaller bones are likely due to a combination of decreased proliferation and increased apoptosis. The cartilage does not appear to be smaller due to effects of the virus at stage 32. It seems that apoptosis is altered in condensing cartilage at younger stages and it is possible that proliferation is also altered at younger stages.

Table 3.7 Quantification of TUNEL positive cells in GFP or CYP26A1 infected embryos at stage 30 and 32

Stage 30 (n=2 GFP, n = 2 CYP26A1)[1]	Virus (# Number of sections):	Level of Apoptosis in each section (TUNEL +tive cells)			
		0 to 5	5 to 10	10 to 15	15 to 20
Cartilage	GFP – L (n = 3)	3	0	0	0
	GFP – R (n = 2)	2	0	0	0
	CYP – L (n = 5)	3	1	1	0
	CYP – R (n = 5)	1	2	1	1
Bone	GFP – L (n = 2)	1	1	0	0
	GFP – R (n = 1)	1	0	0	0
	CYP – L (n = 5)	4	1	0	0
	CYP – R (n = 5)	4	0	1	0
Stage 32 (n=3)					
Cartilage	GFP – L (n = 9)	9	0	0	0
	GFP – R (n = 9)	6	3	0	0
	CYP – L (n = 6)	6	0	0	0
	CYP – R (n = 5)	5	0	0	0
Bone	GFP – L (n = 7)	5	2	0	0
	GFP – R (n = 10)	9	1	0	0
	CYP – L (n = 6)	2	1	3	0
	CYP – R (n = 6)	1	1	2	2

[1]For each embryo, up to 10 sections (technical replicates) were analyzed for TUNEL. Discrepancies in the number of technical replicates between each treatment were due to damaged sections

Chapter 4 - Discussion

Little is known about the effect of RA deficiency later in development as a systemic lack of RA causes early embryo death. This study has developed a means to locally decrease RA by over expression of the catabolic enzyme CYP26A1. My results show that embryos can survive easily until full skeletal differentiation has taken place. I have therefore been able for the first time to assess the role of RA in skeletal development in localized areas targets, in vivo.

4.1 RA is required for bone and cartilage development in a stage but not position specific manner

One of the key results of my work is that there is a stage dependent response to lowering the levels of RA. Embryos were infected at different stages, thereby controlling the time at which *CYP26A1* is expressed relative to the onset of skeletal differentiation. This is not as easily achieved in the mouse model. There is a window between stage 15 and 20 when facial development is sensitive to RA signaling. During this period, molecular events determine which neural crest cells will contribute to bone and cartilage formation. After stage 20, the cells are committed to skeletal formation and RA levels can no longer change their fate.

The lack of position specific effects was somewhat surprising in view of the highly localized patterning effects of RA beads in the face. Excess RA causes truncation of the frontonasal mass (Richman and Delgado, 1995; Tamarin et al., 1984) and RA combined with Noggin transforms just the maxillary prominence (Lee et al., 2001) and not other regions of the face (unpublished data, Richman lab). The difference between these results and mine is that I have shown a minimum level of RA is needed for normal development. The patterning effects of exogenous RA may work via different mechanisms.

4.2 Meckel's cartilage is reduced due to increased apoptosis

Meckel's cartilage was significantly reduced in size in the CYP26A1 injected embryos and this effect was seen starting at stage 30, the earliest stage at which the skeleton was evaluated in this study. We accept the hypothesis that increased apoptosis was in part responsible for the smaller cartilage and that this occurred at stage 30 if not earlier. We did not examine proliferation in stage 30 embryos therefore we cannot exclude a fundamental problem with outgrowth of the mesenchyme and/or a decrease in proliferation in the condensing cartilage. By the time we examined the proliferation at stage 32, there was no longer active proliferation in Meckel's cartilage. It is also possible that if embryos were injected at stage 10 instead of stage 15, more profound effects on all the cartilages in the head might have been observed. In the present dataset, there were minimal effects on the midline cartilages of the upper beak. This may be due to these cartilages being specified earlier in development.

4.3 RA is required for a stage specific expansion of intramembranous bone condensations

The CYP26A1 virus inhibited the differentiation of membranous bone formation in all regions of the head. The detailed analysis of one of these bones, the angular at stage 30 and 32 showed that apoptosis increased but this was only apparent at stage 32. Proliferation was also decreased at stage 32. We did not examine proliferation in detail however it does appear that at stage 32 both decreased proliferation and increased apoptosis are reducing the size of the bone condensations It seems that *CYP26A1* has a repressive effect on the intramembranous bones and that this occurs later than for cartilage.

None of the other loss-of-function studies in which RA signaling was reduced focused on differentiation of the craniofacial skeleton. They were more concerned with patterning of the skeleton in the case of compound RAR knockouts (Lohnes et al, 1994), or with early truncation of the face in the *Raldh2* knockouts. The one exception is the work from our lab in which Citral-soaked beads were implanted into the stage 20 nasal pit (Song et al 2004). Citral a chemical antagonist of RALDH but is not

specific to just this pathway. Similar to the embryos injected in the frontonasal mass with *CYP26A1*, embryos treated with Citral-soaked beads in the nasal pit had dramatic phenotype with large clefts accompanied by reduced or missing intramembranous bones. In addition to the effects on bones, the Citral treated embryos also had reduced cartilage, which was not seen in the CYP26A1 infected embryos. However, Citral treatment resulted in a large amount of apoptosis which was the likely cause of the dramatic phenotype. In comparison, CYP26A1 infection caused a localized increase in apoptosis, as shown by my TUNEL analysis. In addition embryos looked relatively normal at younger stages. Thus the phenotype that we see is not due to a general deficiency in mesenchymal cells in general, but rather is due mainly to the inhibition of bone differentiation.

4.4 CYP26A1 overexpression reduces but does not completely eliminate RA activity

The reduction in RA activity is presumed based on the slight decrease in *RARβ* expression in several embryos. In addition this study showed that *RALDH2* is reduced in the majority of *CYP26A1*-infected embryos. It is straightforward to explain the effects on *RARβ* in which direct regulation by RA is known. The presence of an RARE in the promoter of *RALDH2* has not been demonstrated. Nonetheless at least one study showed that RA is capable of inducing RALDH2 (Maden, 2007). Therefore our data is showing decreased expression of *RALDH2* consistent with endogenous RA levels being reduced. Furthermore, the luciferase data tests suggest that exogenous RA, CYP26A1 can reduce RA signaling activity. This in vitro test did not however show a clear effect.

Another puzzling result was the lack of change in 8 of the expected downstream targets of RA signaling (*BMP4, BMP7, BAMBI, MSX1, MSX2, MEIS2, PITX2, and FGF8*). This may be due to the fact that wholemount in situ hybridization is not sensitive enough to detect the small changes in gene expression. The levels of expression of these genes may be reduced to a lesser extent since all are indirect targets of RA.

Other approaches need to be used to support the premise that the CYP26A1 virus had indeed reduced the level of RA in the tissues. QPCR could be used to quantify gene expression changes. This method could potentially reveal small changes in expression not seen in the wholemount in situ. A second idea is to attempt to rescue the CYP26A1 phenotype (which is very reproducible) by adding RA to the egg. Here, the prediction is that RA addition should rescue the mandibular defects while also causing a specific upper beak truncation (Tamarin, 1984).

Finally we need to consider that some of the effects of the CYP26A1 virus could be due to alteration in the levels of RA metabolites or to change in the expression of endogenous CYP genes. The increase in RA has been shown to increase the level of metabolites created by CYP26 enzymes including 4-oxo-RA, 4-OH-RA, 18-OH-RA and 5,6-epoxy-RA (White et al., 1997). Thus by increasing the level of CYP26A1 the levels of these metabolites should have increased. Other studies have shown that the implantation of beads soaked in the metabolites increases expression of *CYP26A1, B1* but downregulates C1 (Reijntjes et al., 2005; Reijntjes et al., 2004). The present study did not examine embryos for *CYP26A, B1* or *C1* expression since there is very little endogenous expression in the head (Reijntjes et al., 2005). It is possible however that at older stages there are new domains of expression acquired. We have seen this in the case of the maxillary expression domain of *RALDH2* which is absent at stage 18 (Blentic, 2003) and does not appear until stage 22. It is possible that in normal embryos CYP26 genes are expressed in the face of older embryos, a possibility that will be examined in the future. In this case the presence of a feedback loop with the endogenous CYP26 genes would be worthwhile examining.

Even though the readouts of RA signaling are not clearly pointing to a decrease in RA activity, the *CYP26A1*-infected embryo may be a type of hypomorph which has a less severe deficiency of RA than that produced by other types of manipulations such as Citral beads, VAD quail, and knockouts of the *Raldh* or *Rar* genes. It is a useful approach to have a partial loss of function since sometimes full loss

of function obscures the function of a pathway or gene. I have learned that RA has specific effects on skeletogenesis through my system (Fig. 4.1). My model is that RA is maintaining the expression of RALDH2 which increases synthesis of RA. The RA is required for cell proliferation in osteogenic condensations and for cell survival in the cartilage.

Figure 4.1 Summary of the role of endogenous RA in skeletogenesis
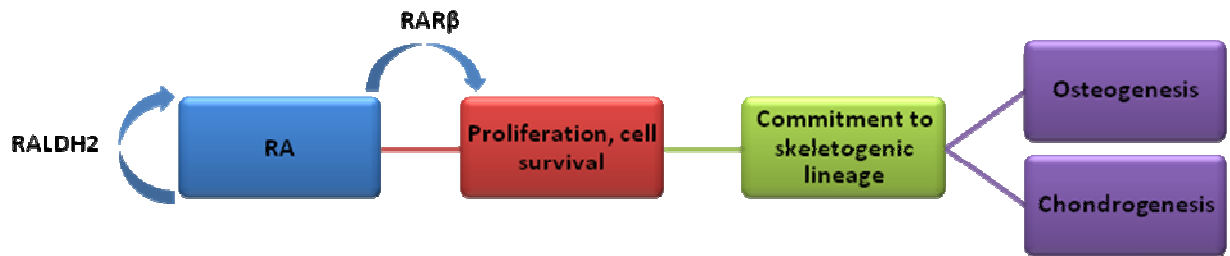

Figure 4.1. Endogenous retinoic acid contributes to skeletogenesis by maintaining cell proliferation in osteogenic condensations and survival in cartilage blastema. RA directly regulating the expression of *RARβ*, which allows the cells to commit to a skeletogenic lineage. RA also self regulates by inducing the expression of its synthesizing enzyme *RALDH2*. Key: RA – retinoic acid

References

Abzhanov, A., Tzahor, E., Lassar, A. B. and Tabin, C. J. (2003). Dissimilar regulation of cell differentiation in mesencephalic (cranial) and sacral (trunk) neural crest cells in vitro. *Development* **130**, 4567-79.

Ashique, A. M., Fu, K. and Richman, J. M. (2002). Endogenous bone morphogenetic proteins regulate outgrowth and epithelial survival during avian lip fusion. *Development* **129**, 4647-60.

Balkan, W., Colbert, M., Bock, C. and Linney, E. (1992). Transgenic indicator mice for studying activated retinoic acid receptors during development. *Proc Natl Acad Sci U S A* **89**, 3347-51.

Balmer, J. E. and Blomhoff, R. (2005). A robust characterization of retinoic acid response elements based on a comparison of sites in three species. *J Steroid Biochem Mol Biol* **96**, 347-54.

Barlow, A. J. and Francis-West, P. H. (1997). Ectopic application of recombinant BMP-2 and BMP-4 can change patterning of developing chick facial primordia. *Development* **124**, 391-398.

Blentic, A., Gale, E. and Maden, M. (2003). Retinoic acid signalling centres in the avian embryo identified by sites of expression of synthesising and catabolising enzymes. *Dev Dyn* **227**, 114-27.

Brown, J. M., Wedden, S. E., Millburn, G. H., Robson, L. G., Hill, R. E., Davidson, D. R. and Tickle, C. (1993). Experimental analysis of the control of expression of the homeobox-gene Msx-1 in the developing limb and face. *Development* **119**, 41-8.

Creuzet, G. C. a. N. L. D. a. S. (2005). Patterning the neural crest derivatives during development of the vertebrate head: insights from avian studies. *J Anat* **207**, 447-459.

Creuzet, S., Couly, G., Vincent, C. and Le Douarin, N. M. (2002). Negative effect of Hox gene expression on the development of the neural crest-derived facial skeleton. *Development* **129**, 4301-13.

de Thé, H., Marchio, A., Tiollais, P. and Dejean, A. (1989). Differential Expression and Ligand Regulation of the Retinoic Acid Receptor-Alpha and Receptor-Beta Genes. *Embo Journal* **8**, 429-433.

Deltour, L., Foglio, M. H. and Duester, G. (1999). Metabolic Deficiencies in Alcohol Dehydrogenase Adh1,Adh3, and Adh4 Null Mutant Mice, vol. 274 (ed., pp. 16796-16801.

Dupe, V., Matt, N., Garnier, J. M., Chambon, P., Mark, M. and Ghyselinck, N. B. (2003). A newborn lethal defect due to inactivation of retinaldehyde dehydrogenase type 3 is prevented by maternal retinoic acid treatment. *Proc Natl Acad Sci U S A* **100**, 14036-41.

Francis, P. H., Richardson, M. K., Brickell, P. M. and Tickle, C. (1994). Bone morphogenetic proteins and a signalling pathway that controls patterning in the developing chick limb. *Development* **120**, 209-18.

Guris, D. L., Duester, G., Papaioannou, V. E. and Imamoto, A. (2006). Dose-dependent interaction of Tbx1 and Crkl and locally aberrant RA signaling in a model of del22q11 syndrome. *Dev Cell* **10**, 81-92.

Halilagic, A., Ribes, V., Ghyselinck, N. B., Zile, M. H., Dollé, P. and Studer, M. (2007). Retinoids control anterior and dorsal properties in the developing forebrain. *Developmental Biology* **303**, 362-375.

Halilagic, A., Zile, M. H. and Studer, M. (2003). A novel role for retinoids in patterning the avian forebrain during presomite stages. *Development* **130**, 2039-50.

Hamburger, V. and Hamilton, H. (1951). A series of normal stages in the development of the chick embryo. *J. Morphol.* **88**, 49-92.

Healy, C., Uwanogho, D. and Sharpe, P. T. (1999). Regulation and role of Sox9 in cartilage formation. *Dev Dyn* **215**, 69-78.

Higashihori, N., Buchtová, M., Fu, K. and Richman, J. M. (2009). TBX22 differentially mediates the effects of FGF and BMP signaling pathways and retroviral misexpression induces orofacial clefting in avian embryos. *Dev Biol* **In revision**.

Higashihori, N., Song, Y. and Richman, J. M. (2008). Expression and regulation of the decoy bone morphogenetic protein receptor BAMBI in the developing avian face. *Dev Dyn* **237**, 1500-8.

Hu, D., Colnot, C. and Marcucio, R. S. (2008). Effect of bone morphogenetic protein signaling on development of the jaw skeleton. *Dev Dyn* **237**, 3727-37.

Kawaguchi, R., Yu, J., Honda, J., Hu, J., Whitelegge, J., Ping, P., Wiita, P., Bok, D. and Sun, H. (2007). A Membrane Receptor for Retinol Binding Protein Mediates Cellular Uptake of Vitamin A, vol. 315 (ed., pp. 820-825.

Kumar, S. and Duester, G. (2011). Retinoic acid signaling in perioptic mesenchyme represses Wnt signaling via induction of Pitx2 and Dkk2. *Dev Biol* **340**, 67-74.

Le Douarin, N. (1969). Particularites du noyau interphasique chez la caille japonaise (Coturnix coturnix japonica), Utilisation de ces particularites comme "marquage biologique" dans des recherches sur les interactions tissulaires et les migrations cellulaires au cours de l'ontogenèse. *Bull. Biol. Fr. Belg.* **103**, 435-542.

Le Douarin, N. M., Creuzet, S., Couly, G. and Dupin, E. (2004). Neural crest cell plasticity and its limits. *Development* **131**, 4637-50.

Lee, S. H., Bedard, O., Buchtova, M., Fu, K. and Richman, J. M. (2004). A new origin for the maxillary jaw. *Dev Biol* **276**, 207-24.

Lee, S. H., Fu, K. K., Hui, J. N. and Richman, J. M. (2001). Noggin and retinoic acid transform the identity of avian facial prominences. *Nature* **414**, 909-912.

Loftus, S. K., Larson, D. M., Watkins-Chow, D., Church, D. M. and Pavan, W. J. (2001). Generation of RCAS Vectors Useful for Functional Genomic Analyses. *DNA Research* **8**, 221-226.

Lohnes, D., Mark, M., Mendelsohn, C., Dolle, P., Dierich, A., Gorry, P., Gansmuller, A. and Chambon, P. (1994). Function of the retinoic acid receptors (RARs) during development (I). Craniofacial and skeletal abnormalities in RAR double mutants. *Development* **120**, 2723-48.

Lufkin, T., Lohnes, D., Mark, M., Dierich, A., Gorry, P., Gaub, M. P., LeMeur, M. and Chambon, P. (1993). High postnatal lethality and testis degeneration in retinoic acid receptor alpha mutant mice, vol. 90 (ed., pp. 7225-7229.

Lumsden, A., Sprawson, N. and Graham, A. (1991). Segmental origin and migration of neural crest cells in the hindbrain region of the chick embryo. *Development* **113**, 1281-91.

MacDonald, M. E., Abbott, U. K. and Richman, J. M. (2004). Upper beak truncation in chicken embryos with the cleft primary palate mutation is due to an epithelial defect in the frontonasal mass. *Dev Dyn* **230**, 335-49.

Maden, M. (2000). The role of retinoic acid in embryonic and post-embryonic development. *Proc Nutr Soc* **59**, 65-73.

Maden, M. (2006a). Retinoids and spinal cord development. *J Neurobiol* **66**, 726-38.

Maden, M. (2006b). Retinoids have differing efficacies on alveolar regeneration in a dexamethasone-treated mouse. *Am J Respir Cell Mol Biol* **35**, 260-7.

Maden, M. (2007). Retinoic acid in the development, regeneration and maintenance of the nervous system. *Nat Rev Neurosci* **8**, 755-65.

Maden, M., Blentic, A., Reijntjes, S., Seguin, S., Gale, E. and Graham, A. (2007). Retinoic acid is required for specification of the ventral eye field and for Rathke's pouch in the avian embryo. *Int J Dev Biol* **51**, 191-200.

Maden, M., Sonneveld, E., van der Saag, P. T. and Gale, E. (1998). The distribution of endogenous retinoic acid in the chick embryo: implications for developmental mechanisms. *Development* **125**, 4133-44.

Matovinovic, E. and Richman, J. M. (1997). Epithelium is required for maintaining FGFR-2 expression levels in facial mesenchyme of the developing chick embryo. *Dev Dyn* **210**, 407-16.

McCaffery, P., Wagner, E., O'Neil, J., Petkovich, M. and Drager, U. C. (1999). Dorsal and ventral retinal territories defined by retinoic acid synthesis, break-down and nuclear receptor expression. *Mech Dev* **82**, 119-30.

McCaffery, P. J., Adams, J., Maden, M. and Rosa-Molinar, E. (2003). Too much of a good thing: retinoic acid as an endogenous regulator of neural differentiation and exogenous teratogen. *Eur J Neurosci* **18**, 457-72.

Mercader, N., Leonardo, E., Piedra, M. E., Martinez, A. C., Ros, M. A. and Torres, M. (2000). Opposing RA and FGF signals control proximodistal vertebrate limb development through regulation of Meis genes. *Development* **127**, 3961-70.

Molotkov, A., Fan, X., Deltour, L., Foglio, M. H., Martras, S. l., Farrés, J., Parés, X. and Duester, G. (2002). Stimulation of retinoic acid production and growth by ubiquitously expressed alcohol dehydrogenase Adh3, vol. 99 (ed., pp. 5337-5342.

Murray, P. D. F. (1963). Adventitious (secondary) cartilage in the chick embryo, and the development of certain bones and articulation in the chick skull. *Aust J Zool* **11**, 368-430.

Niederreither, K., Abu-Abed, S., Schuhbaur, B., Petkovich, M., Chambon, P. and Dolle, P. (2002a). Genetic evidence that oxidative derivatives of retinoic acid are not involved in retinoid signaling during mouse development. *Nat Genet* **31**, 84-8.

Niederreither, K. and Dolle, P. (2008). Retinoic acid in development: towards an integrated view. *Nat Rev Genet* **9**, 541-53.

Niederreither, K., Fraulob, V., Garnier, J. M., Chambon, P. and Dolle, P. (2002b). Differential expression of retinoic acid-synthesizing (RALDH) enzymes during fetal development and organ differentiation in the mouse. *Mech Dev* **110**, 165-71.

Niederreither, K., McCaffery, P., Dräger, U. C., Chambon, P. and Dollé, P. (1997). Restricted expression and retinoic acid-induced downregulation of the retinaldehyde dehydrogenase type 2 (RALDH-2) gene during mouse development. *Mech Dev* **62**, 67-78.

Niederreither, K., Vermot, J., Fraulob, V., Chambon, P. and Dolle, P. (2002c). Retinaldehyde dehydrogenase 2 (RALDH2)- independent patterns of retinoic acid synthesis in the mouse embryo. *Proc Natl Acad Sci U S A* **99**, 16111-6.

Niederreither, K., Vermot, J., Schuhbaur, B., Chambon, P. and Dolle, P. (2002d). Embryonic retinoic acid synthesis is required for forelimb growth and anteroposterior patterning in the mouse. *Development* **129**, 3563-74.

Quinlan, R., Gale, E., Maden, M. and Graham, A. (2002). Deficits in the posterior pharyngeal endoderm in the absence of retinoids. *Dev Dyn* **225**, 54-60.

Reijntjes, S., Blentic, A., Gale, E. and Maden, M. (2005). The control of morphogen signalling: regulation of the synthesis and catabolism of retinoic acid in the developing embryo. *Dev Biol* **285**, 224-37.

Reijntjes, S., Gale, E. and Maden, M. (2004). Generating gradients of retinoic acid in the chick embryo: Cyp26C1 expression and a comparative analysis of the Cyp26 enzymes. *Dev Dyn* **230**, 509-17.

Reijntjes, S., Rodaway, A. and Maden, M. (2007). The retinoic acid metabolising gene, CYP26B1, patterns the cartilaginous cranial neural crest in zebrafish. *Int J Dev Biol* **51**, 351-60.

Reijntjes, S., Zile, M. H. and Maden, M. (2010). The expression of Stra6 and Rdh10 in the avian embryo and their contribution to the generation of retinoid signatures.

Ribes, V., Fraulob, V., Petkovich, M. and Dolle, P. (2007). The oxidizing enzyme CYP26a1 tightly regulates the availability of retinoic acid in the gastrulating mouse embryo to ensure proper head development and vasculogenesis. *Dev Dyn* **236**, 644-53.

Richany, S. F., Bast, T. H. and Angevine, D. M. (1959). Localization of alkaline phosphatase in the histogenesis of cartilage and bone. *J Bone Joint Surg Am* **41-A**, 939-47.

Richman, J. M. and Crosby, Z. (1990). Differential growth of facial primordia in chick embryos: responses of facial mesenchyme to basic fibroblast growth factor (bFGF) and serum in micromass culture. *Development* **109**, 341-8.

Richman, J. M. and Delgado, J. L. (1995). Locally released retinoic acid leads to facial clefts in the chick embryo but does not alter the expression of receptors for fibroblast growth factor. *J Craniofac Genet Dev Biol* **15**, 190-204.

Richman, J. M. and Tickle, C. (1989). Epithelia are interchangeable between facial primordia of chick embryos and morphogenesis is controlled by the mesenchyme. *Dev Biol* **136**, 201-10.

Roberts, C., Ivins, S., Cook, A. C., Baldini, A. and Scambler, P. J. (2006). Cyp26 genes a1, b1 and c1 are down-regulated in Tbx1 null mice and inhibition of Cyp26 enzyme function produces a phenocopy of DiGeorge Syndrome in the chick. *Hum Mol Genet* **15**, 3394-410.

Rodriguez-Leon, J., Merino, R., Macias, D., Ganan, Y., Santesteban, E. and Hurle, J. M. (1999). Retinoic acid regulates programmed cell death through BMP signalling. *Nat Cell Biol* **1**, 125-6.

Romanoff, A. (1960). The Avian Embryo. Structural and Functional Development. New York: Macmillan Company.

Rossant, J., Zirngibl, R., Cado, D., Shago, M. and Giguere, V. (1991). Expression of a retinoic acid response element-hsplacZ transgene defines specific domains of transcriptional activity during mouse embryogenesis. *Genes Dev* **5**, 1333-44.

Rowe, A., Richman, J. M. and Brickell, P. M. (1991). Retinoic acid treatment alters the distribution of retinoic acid receptor-beta transcripts in the embryonic chick face. *Development* **111**, 1007-16.

Rowe, A., Richman, J. M. and Brickell, P. M. (1992). Development of the spatial pattern of retinoic acid receptor-beta transcripts in embryonic chick facial primordia. *Development* **114**, 805-13.

Sakai, Y., Luo, T., McCaffery, P., Hamada, H. and Drager, U. C. (2004). CYP26A1 and CYP26C1 cooperate in degrading retinoic acid within the equatorial retina during later eye development. *Dev Biol* **276**, 143-57.

Sakai, Y., Meno, C., Fujii, H., Nishino, J., Shiratori, H., Saijoh, Y., Rossant, J. and Hamada, H. (2001). The retinoic acid-inactivating enzyme CYP26 is essential for establishing an uneven distribution of retinoic acid along the anterio-posterior axis within the mouse embryo. *Genes Dev* **15**, 213-25.

Schneider, R. A., Hu, D., Rubenstein, J. L., Maden, M. and Helms, J. A. (2001). Local retinoid signaling coordinates forebrain and facial morphogenesis by maintaining FGF8 and SHH. *Development* **128**, 2755-67.

Semba, I., Nonaka, K., Takahashi, I., Takahashi, K., Dashner, R., Shum, L., Nuckolls, G. H. and Slavkin, H. C. (2000). Positionally-dependent chondrogenesis induced by BMP4 is co-regulated by sox9 and msx2. *Developmental Dynamics* **217**, 401-414.

Song, Y., Hui, J. N., Fu, K. K. and Richman, J. M. (2004). Control of retinoic acid synthesis and FGF expression in the nasal pit is required to pattern the craniofacial skeleton. *Dev Biol* **276**, 313-29.

Stoppie, P., Borgers, M., Borghgraef, P., Dillen, L., Goossens, J., Sanz, G., Szel, H., Van Hove, C., Van Nyen, G., Nobels, G. et al. (2000). R115866 inhibits all-trans-retinoic acid metabolism and exerts retinoidal effects in rodents. *J Pharmacol Exp Ther* **293**, 304-12.

Stratford, T., Horton, C. and Maden, M. (1996). Retinoic acid is required for the initiation of outgrowth in the chick limb bud. *Curr Biol* **6**, 1124-33.

Suzuki, R., Shintani, T., Sakuta, H., Kato, A., Ohkawara, T., Osumi, N. and Noda, M. (2000). Identification of RALDH-3, a novel retinaldehyde dehydrogenase, expressed in the ventral region of the retina. *Mech Dev* **98**, 37-50.

Szabo-Rogers, H. L., Geetha-Loganathan, P., Nimmagadda, S., Fu, K. K. and Richman, J. M. (2008). FGF signals from the nasal pit are necessary for normal facial morphogenesis. *Dev Biol* **318**, 289-302.

Szabo-Rogers, H. L., Geetha-Loganathan, P., Whiting, C. J., Nimmagadda, S., Fu, K. and Richman, J. M. (2009). Novel skeletogenic patterning roles for the olfactory pit. *Development* **136**, 219-29.

Tahayato, A., Dolle, P. and Petkovich, M. (2003). Cyp26C1 encodes a novel retinoic acid-metabolizing enzyme expressed in the hindbrain, inner ear, first branchial arch and tooth buds during murine development. *Gene Expr Patterns* **3**, 449-54.

Tamarin, A., Crawley, A., Lee, J. and Tickle, C. (1984). Analysis of upper beak defects in chicken embryos following with retinoic acid. *J Embryol Exp Morphol* **84**, 105-23.

Tay, S., Dickmann, L., Dixit, V. and Isoherranen, N. (2009). A Comparison of the Role of PPAR and RAR on CYP26 Regulation, (ed., pp. -.

Theodosiou, M., Laudet, V. and Schubert, M. (2010). From carrot to clinic: an overview of the retinoic acid signaling pathway. *Cellular and Molecular Life Sciences* **67**, 1423-1445.

Tickle, C., Alberts, B., Wolpert, L. and Lee, J. (1982). Local application of retinoic acid to the limb bond mimics the action of the polarizing region. *Nature* **296**, 564-6.

Tickle, C., Lee, J. and Eichele, G. (1985). A quantitative analysis of the effect of all-trans-retinoic acid on the pattern of chick wing development. *Dev Biol* **109**, 82-95.

Tosney, K. W. (1982). The segregation and early migration of cranial neural crest cells in the avian embryo. *Dev Biol* **89**, 13-24.

Wagner, M., Han, B. and Jessell, T. M. (1992). Regional differences in retinoid release from embryonic neural tissue detected by an in vitro reporter assay. *Development* **116**, 55-66.

Wasiak, S. and Lohnes, D. (1999). Retinoic acid affects left-right patterning. *Dev Biol* **215**, 332-42.

Wedden, S. E., Lewin-Smith, M. R. and Tickle, C. (1986). The patterns on chondrogenesis of cells from facial primordia of chick embryos in micromass culture. *Dev Biol* **117**, 71-82.

Wedden, S. E., Lewin-Smith, M. R. and Tickle, C. (1987). The effects of retinoids on cartilage differentiation in micromass cultures of chick facial primordia and the relationship to a specific facial defect. *Dev Biol* **122**, 78-89.

Weston, A. D., Blumberg, B. and Underhill, T. M. (2003). Active Repression by Unliganded Retinoid Receptors in Development: Less Is Sometimes More. *J Cell Biol* **161**, 223-228.

White, J. A., Beckett-Jones, B., Guo, Y. D., Dilworth, F. J., Bonasoro, J., Jones, G. and Petkovich, M. (1997). cDNA cloning of human retinoic acid-metabolizing enzyme (hP450RAI) identifies a novel family of cytochromes P450. *J Biol Chem* **272**, 18538-41.

Wilson, L., Gale, E., Chambers, D. and Maden, M. (2004). Retinoic acid and the control of dorsoventral patterning in the avian spinal cord. *Dev Biol* **269**, 433-46.

Zanotti, G., Berni, R. and Gerald, L. (2004). Plasma Retinol-Binding Protein: Structure and Interactions with Retinol, Retinoids, and Transthyretin. In *Vitamins & Hormones*, vol. Volume 69, pp. 271-295: Academic Press.

Zernik, J., Twarog, K. and Upholt, W. B. (1990). Regulation of alkaline phosphatase and alpha 2(I) procollagen synthesis during early intramembranous bone formation in the rat mandible. *Differentiation* **44**, 207-15.

Appendix 1

Whole-mount *in situ* hybridization

1. Dissect chick embryos in ice cold PBS. Remove as much of extra-embryonic membranes as possible for stages > 10. Tear the mesencephalons to allow easier access of probe penetration.

2. Fix in 4% PFA for 1-2 hrs at RT or 4°C overnight.

3. Dehydrate the embryos. The washing time depends on the stage of embryos. Put on rotor.

        2X in PTW (PBS + 0.1% Tween20)

        50% MeOH/PTW

        2 X in 100% MeOH

4. Store at -20°C.

DAY 1 Pretreatment and hybridization

5. Rehydrate embryos through   75% MeOH/PTW

                                 50% MeOH/PTW

                                 25% MeOH/PTW

Let settle each time.

6. Wash 2X in PTW for 5 minutes each.

7. Treat with 10 ug/ml or 20 ug/ml proteinase K (diluted in PTW) with specific time depending on the stage of the embryos and the kind of probe. The goal is to increase the accessibility of target RNA, thereby improving the signal. **USE DEPC tx water from now on until the end of Day 1.**

8. Quickly rinse with PTW (embryos are especially fragile after proteinase K treatment, handle with extra care!). Post-fix for 20 minutes in 4% PFA+0.1% glutaraldehyde(made in PTW) at RT.

9. Rinse with PTW. Wash for 5 minutes in PTW. Transfer embryos to 2 ml screw cap microtubes.

10. Rinse with 1: 1 PTW/hybridization mix. Invert tube and let settle. Avoid air bubbles.

Hybridization mix: Deionized formamide   25 ml

                         20X SSC, **pH 4.5**   3.25 ml

                         0.5M EDTA, pH 8.0   0.5 ml

                         20mg/ml Yeast TRNA   125 ul

                         10% Tween-20   1 ml

                         10% CHAPS   2.5 ml

                         50 mg/ml Heparin   100 ul

DEPC H$_2$0	17.5 ml
Total	50 ml.

11. Rinse briefly with hybridization mix and let settle. Embryos become quite transparent in formamide soln, take extra care not to accidentally discard them.

12. Add 2 ml of hybridization mix to each tube and incubate at 70°C on rotor for 1 hr minimum. Avoid air bubbles. Prewarm the hybridization mix in 70°C heat block.

13. Add 10 ul of the corresponding probe to 1.5 ml prewarmed hybridization mix for each new microtube on the 70°C heat block. Take samples out of 70°C oven rotor, remove soln and add the RNA/hybrid mix solution to the corresponding samples **quickly**. A constant temperature of 70°C is critical for this step to keep hybridization efficiency and decrease background nonspecific binding.

14. Leave samples in 70°C oven rotor and hybrid mix in 70°C heat block overnight.

DAY 2 Post-hybridization washes to remove probe that has not annealed to target RNA and antibody incubation. USE regular ddH$_2$O for Day 2 and Day 3. No need for DEPC tx water since nothing needs to be RNAse free from this point onwards.

1. Transfer RNA/hybrid mix solution to new 2 ml screw cap tubes. Quickly dry freeze them or immediately put in -80°C to preserve quality of probe. Rinse 2 X with prewarmed hybridization mix (70°C).

2. Wash 2 X 30 minutes with prewarmed hybridization mix (70°C) on rotor.

3. Wash 10 minutes with prewarmed 1: 1 hybridization mix/MABT (70°C) on rotor.

    5X MAB

Maleic Acid	0.5 M	58.04 g
NaCl	0.75 M	43.83 g
DEPC-H$_2$O		to 1 L

    (pH to 7.5 using NaOH pellets, note a precipitate will form around pH 2-5 but it will go back into solution when it gets to 7.5)

    MABT:

5X MAB	dilute to 1 X MAB
10% Tween-20	dilute to **0.1%** Final conc
DEPC H$_2$0	

4. Rinse 2 X with MABT at RT.

5. Wash in MABT for 15 minutes at RT on rotor.

6. Incubate 1 hr with MABT + 2% Boehringer Blocking Reagent (BBR) at RT on rotor.

    Freshly made:

DEPC H$_2$0	1.58 ml
5X MAB + 10% BBR	400 ul
10% Tween-20 (**0.1%** Final conc)	20 ul Total 2 ml for **each** microtube.

7. Incubate 1 hr or more with MABT + 2% BBR + 20% HISS at RT on rotor to prevent nonspecific binding of antibody.

    Freshly made:

DEPC H$_2$0	1.18 ml
5X MAB + 10% BBR	400 ul
10% Tween-20 (**0.1%** Final conc)	20 ul
HISS	400 ul Total 2 ml for **each** microtube.

8. Incubate overnight in MABT+ 2% BBR + 20% HISS + 1/2000 anti-DIG AP Ab fragment (Boehringer) at 4°C on rotor.

    Freshly made:

DEPC H$_2$0	1.179 ml
5X MAB + 10% BBR	400 ul
10% Tween-20 (**0.1%** Final conc)	20 ul
HISS	400 ul
Anti-DIG Ab	1 ul Total 2 ml for **each** microtube.

DAY 3 Post Ab washes to remove unbound Ab and histochemistry

1. Rinse 3 X with MABT (**1% Tween-20**).

    DEPC H$_2$0

    5XMAB   dilute to 1X MAB

    10% Tween-20   dilute to **1%** Final conc

2. Transfer to 4 ml glass scintillation vials since a precipitate can form if histochemical reaction is carried out in a plastic container. Wash 3 X in MABT for 1 hr each on rotor.

3. Wash 2 X in NTMT for 10 minutes each on rotor.

5 M NaCl	1 ml
1 M TrisHCl **pH 9.5**	5 ml
2 M MgCl$_2$	1.25 ml

        10% Tween-20(**1%** Final conc)   5 ml

        DEPC H$_2$0   37.75 ml   Total 50 ml

4. Incubate with NTMT+ 4.5 ul/ml NBT + 3.5 ul/ml BCIP at 4°C in dark film container. No rolling. Monitor the reaction at intervals under a dissecting microscope. It is important to obtain a maximal signal strength but not to allow the backgrounds to become unacceptably high.

NBT:

75 mg/ml Nitro blue tetrazolium in 70% dimethyl formamide and 30% water

BCIP:

50 mg/ml 5-bromo-4-chloro-3-indoyl phosphate in 100% dimethyl formamide

5. Stop reaction by rinsing the embryos with PTW (Can keep embryos in PTW at 4°C for a while before refixing. If signal is not good enough, go back to step 3). Then refix the embryos in 10% formalin in 1.5 ml eppendorfs. Store at RT.